Towards a tailored therapeutic approach for vulvar cancer patients

Kortekaas, K.E.

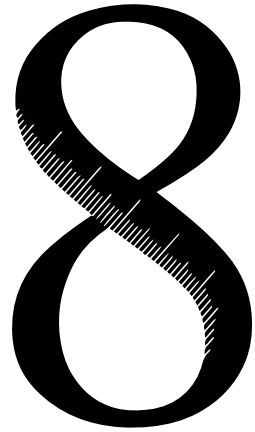

CD39 IDENTIFIES THE CD4-POSITIVE TUMOR-SPECIFIC T CELL POPULATION IN HUMAN CANCER

K.E. Kortekaas*, S.J.A.M. Santegoets*, G. Sturm, I. Ehsan, S.L. van Egmond, F. Finotello, Z. Trajanoski, M.J.P. Welters, M.I.E. van Poelgeest, S.H. van der Burg

*These authors contributed equally to this work

Cancer Immunology Research 2020

ABSTRACT

Objective

The accumulation of tumor-specific $CD4^+$ and $CD8^+$ effector T cells is key to an effective anti-tumor response. Locally, $CD4^+$ T cells promote the recruitment and effector function of tumor-specific $CD8^+$ T cells as well as activate innate killer cells in the tumor. Here, we show that also tumor-specific $CD4^+$ T cells are predominantly present in the $CD39^+$ subset of tumor-infiltrating lymphocytes (TIL). The $CD39^+$ $CD4^+$ and $CD8^+$ TIL were detected in three different tumor types, and displayed an activated (PD-1^+, HLA-DR^+) effector memory phenotype. $CD4^+CD39^+$ single cell RNA sequenced TIL shared similar well-known activation, tissue residency, and effector cell-associated genes with $CD8^+CD39^+CD103^+$ TIL. Finally, analysis of directly *ex-vivo* cell sorted and *in vitro* expanded pure populations of CD39-positive and negative $CD4^+$ and $CD8^+$ TIL revealed that tumor-specific antigen reactivity was almost exclusively detected among $CD39^+$ cells.

Synopsis

Immunotherapy of cancer is based on the activation of tumor-reactive $CD4^+$ and $CD8^+$ T cells. Here we show that the expression of CD39 can be utilized to identify, isolate and expand the tumor-reactive T-cell population present in cancers.

INTRODUCTION

In many types of cancer the concerted action of high numbers of effector memory cytotoxic $CD8^+$ T cells and type-1 $CD4^+$ T cells is associated with better prognosis [1, 2] and response to immunotherapy.[3] $CD4^+$ T cells can activate tumor-infiltrating tumoricidal eosinophils, macrophages and natural killer (NK) cells [4-7] as well as promote the recruitment and cytolytic function of $CD8^+$ T cells.[8] In the tumor microenvironment (TME), $CD8^+$ T cells can specifically recognize and kill tumor cells.[9] IFN-γ produced by both subpopulations of T cells is known to enhance MHC class I and II antigen presentation in tumor cells, thereby making them more vulnerable to $CD4^+$ and $CD8^+$ T cell attack. Furthermore, IFN-γ exerts direct anti-proliferative and pro-apoptotic antitumor effects.[10]

Previous work revealed that not all intratumoral T cells respond to tumor antigens[11, 12], because ongoing inflammation also attracts so-called activated bystander T cells, which recognize antigens unrelated to cancer.[11] A more accurate identification of the actual tumor-reactive T cell population not only allows for better interpretation of the potential interactions within the TME, but it may also serve immunotherapy. For instance, to yield higher percentages of tumor-specific T cells in adoptive cell therapy (ACT) approaches, either by direct expansion and infusion of isolated T cells or by using gene-modified T cells expressing the T cell receptor (TCR) of the isolated tumor-reactive T cells. A number of groups isolated tumor-reactive T cells directly from TIL based on the transient expression of CD137 for recently activated T cells[13-15] or on the expression of PD-1[16] as this was predominantly present on highly expanded TCRβ clonotypes.[17] The expression of PD-1 and many other co-inhibitory, co-stimulatory and activation markers is not exclusive for tumor-reactive T cells among T cells in the TME[13, 18] and therefore, not directly useful for the isolation of tumor-reactive T cells. The use of enhanced phenotype definition may overcome such limitations.[19] More recently, CD39 has been proposed as a marker to identify tumor-reactive $CD8^+$ T cells.[11, 18, 20] CD39 expression was detected on $CD8^+$ T cells with hallmarks of chronic antigenic stimulation at the tumor site[11] and correlated with important clinical beneficial parameters in colorectal cancer, lung cancer and head and neck cancer.[11, 18]

Tumor-reactive $CD4^+$ T cells are required for the control of tumor progression in mice[2, 4, 21] and mediate direct effects in patients with cancer.[22-24] CD39 is an ectonucleotidase that becomes expressed at the cell surface of not only activated $CD8^+$ T cells but also on activated $CD4^+$ T cells, and it is retained long after other markers of activation (e.g. CD25, HLA-DR) have perished.[25] As such, the possibility exists that CD39 may also identify tumor-reactive $CD4^+$ TIL. To answer this question, we studied their presence in squamous cell carcinomas of the vulva, oropharynx, and cervix. This provided us with the advantage that a substantial fraction of these tumors was induced by high-risk human papillomavirus (HPV), expressed the known tumor-specific proteins E6 and E7, and were infiltrated by $CD4^+$ and $CD8^+$ TIL

responding to these antigens.[26, 27] Moreover, the detection of HPV-reactive $CD4^+$ T cells among TIL is associated with significantly improved clinical benefit in these cancers.[26] Here, we show that a significant fraction of the $CD4^+$ and $CD8^+$ TIL express CD39. The $CD4^+CD39^+$ cells within these TIL exhibit a tissue-resident/activation-like phenotype similar to that of $CD8^+CD39^+CD103^+$ TIL and the $CD39^+$ TIL almost exclusively comprise the tumor-specific T cell fraction. These results provide a second rationale to focus on CD39 as a marker for the identification and isolation of tumor-specific T cells and will spur the development of effective T-cell based immunotherapies.

METHODS

Patients

Patients included in this study, were part of two larger observational studies focusing on circulating and local immune responses in either anogenital lesions (P08.197) or head and neck cancer (P07.112).[26] Patients were included after histopathology confirmed the presence of a carcinoma and after signing informed consent. The study was conducted in accordance with the Declaration of Helsinki and approved by the local medical ethical committee of Leiden University Medical Center and in agreement with the Dutch law. The materials were used according to the Dutch Federal of Medical Research Association guidelines. All patients received standard-of-care treatment. HPV typing and $p16^{ink}$4a-immunohistochemistry was performed on formalin-fixed paraffin-embedded (FFPE) material as described previously.[27]

Single cell tumor cell digests

Tumor material was obtained after surgery and handled as described.[26] The tumor was cut in small pieces, and subsequently incubated for 15 minutes at 37°C in IMDM dissociation mixture containing 10% human AB serum, high dose of antibiotics, and 0.38 mg/ml of Liberase (Liberase TL, research grade, Roche). After 15 minutes the cell suspension was flushed through a 70 µm cell strainer (Falcon, Durham, NC, USA) to acquire a single cell suspension, counted using trypan blue exclusion (Sigma, St Louis, MO, USA), and cryopreserved at approximately 2 million cells/vial. All cells were stored in the vapor phase of liquid nitrogen until further use.

Flow cytometry of ex vivo tumors

Cryopreserved single cell tumor samples (*n*=30; 10 cervical carcinoma, 9 vulvar squamous cell carcinoma, and 11 oropharyngeal squamous cell carcinoma) were thawed and assessed by flow cytometry as described previously.[28] Briefly dead cells were identified using the LIVE-DEAD Fixable yellow dead cell stain kit (ThermoFisher Scientific) for 20 minutes at room temperature. After incubation, cells were washed and incubated with PBS/0.5%BSA/10%FCS for 15 minutes on ice for FC receptor blockade. Following washing, the cells were stained for 30 minutes on ice in the dark with fluorochrome-conjugated antibodies (supplemental table 1). Acquisition of stained cells was performed with a BD LSR Fortessa. Data was analyzed

by high-dimensional single cell data analysis using hierarchical Stochastical Neighbor Embedding (HSNE) in Cytosplore[29], by clustering using a self-organizing map (FlowSOM) in Cytobank or by manual gating using DIVA software (version 8.02; BD Biosciences).

Single cell RNA sequencing and data analysis

Live CD3$^+$ T cells were isolated from thawed single cell tumor samples using the dead cell removal kit (Miltenyi biotec) followed by CD3-guided magnetic cell sorting using CD3-microbeads (miltenyi biotec) according to manufacturer's instructions. Post-isolation viability was >70%. Single-cell RNA-sequencing was performed as described previously with some modifications.[30] Briefly, cells combined with oil, reagents, and beads were loaded on a Chromium Single Cell Controller (10x Genomics). Lysis and barcoded reverse transcription of polyadenylated mRNA from single cells were performed inside each gel bead emulsion using the 5' gene expression pipeline. Next-generation sequencing libraries were prepared in a single bulk reaction, and transcripts were sequenced using a HiSeq4000 System (Illumina). Single-cell transcriptome sequencing data were preprocessed with cellranger v3.0.0 (10x Genomics) using the GRCh38 reference genome. Downstream analysis was performed using scanpy v1.4.4[31] following the best practice recommendations by Luecken et al.[32] All scripts used to perform the analysis are wrapped into a fully reproducible Nextflow pipeline [10.1038/nbt.3820] and publicly available from GitHub (https://github.com/icbi-lab/kortekaas2020_paper). The data analysis reports including the full list of differentially expressed genes, are available on https://icbi-lab.github.io/kortekaas2020_paper). In brief, low quality cells were excluded by retaining only cells with I) >700 detected genes, II) > 200 detected reads, and III) <11% mitochondrial reads. *In silico* doublet detection was performed with *scrublet v0.2.1*.[33] Finally, 3000 most highly-variable genes (HVGs) were selected and clustered unsupervised using the Leiden algorithm.[34] Embeddings were visualized using UMAP.[35] Differential gene expression between clusters was computed using edgeR.[36] The whole scRNA sequencing data set is available upon reasonable written request without restrictions.

Cell sorting and T cell expansion

Cryopreserved single cell tumor samples were thawed, and stained for dead cells and surface markers CD4, CD8, CD39, and CD103 (supplemental table 1) as described above. Antibodies to CD3 were not used for cell sorting.[18] CD4$^+$CD39$^-$, CD4$^+$CD39$^+$, CD8$^+$CD39$^-$ CD103$^+$, and CD8$^+$CD39$^+$CD103$^+$ populations were sorted using a BD FACSAria III. When sufficient number of cells were obtained, a purity check was performed. Next, the sorted cells were cultured in a 96 wells-plate (20.000 TILs/well), with irradiated PBMC of five different donors (100.000 cells/96 well total) and EBV-transformed B-lymphoblast cell lines of three different donors (10.000 cells/96 well total) in IMDM medium (Gibco by Life technologies, ThermoFisher Scientific, Lonza, Verviers, Belgium) with 10% FCS (PAA laboratories, Pasching, Austria) and 100 IU/mL penicillin, 100 µg/mL streptomycin, 2 mmol/L L-glutamin (Gibco by Life technologies, ThermoFischer Scientific) supplemented with 10% TCG-F (ZeptoMetrix

Corporation, Buffalo, NY, USA), 5 ng/ml human IL-7 (peprotech, London, UK), 5 ng/ml human IL-15 (Invitrogen by ThermoFisher Scientific), 5 ng/ml human IL-21 (generously provided by AIMM Therapeutics), and anti-CD3/CD28 Dynabeads (Gibco by Life technologies, ThermoFisher Scientific) at a PBMC:beads ratio of 3:1. Every 2-3 days, the cultures were replenished with IMDM complete medium supplemented with 10% TCG-F, 5ng/ml of IL-7, IL-15, and IL-21. After 3 weeks, the cultures were harvested, anti-CD3/CD28 Dynabeads were removed, and cells were counted using trypan blue exclusion. Per condition 400.000 cells were stimulated for a second expansion round as described above. The remaining cells were stored in the vapor phase of liquid nitrogen until further use (expansion round 1). Three weeks later, the cultures were harvested, Dynabeads were removed and cells were stored in the vapor phase of liquid nitrogen until further use (expansion round 2).

Tumor-specific T cell reactivity analysis

The presence of HPV-specific T cells was tested by assessment of antigen-specific cytokine production as described previously.[26] T cell responses against autologous HPV16 E6/E7 synthetic long peptide (SLP; 22-mers with 14 amino acids overlap) loaded monocytes were tested in triplicate. PHA (0.5 ug/ml; HA16 Remel; ThermoFisher Scientific) served as a positive control, while unloaded monocytes served as negative controls. At day 1.5 and 4 supernatant (50µl/well) was harvested for cytokine analyses. The antigen-specific cytokine production in the supernatants was determined by cytometric bead array (CBA, Th1/Th2 kit, BD Bioscience, Breda, the Netherlands) according to the manufacturer's instructions. The cut-off value for cytokine production was 20 pg/ml, except for IFN-γ for which it was 40 pg/ml. Antigen-specific cytokine production was defined as at least twice above that of the unstimulated cells.

Statistical analysis

A repeated measure one-way ANOVA with Tukey's multiple comparison was used to determine significant difference in numerical data between four subpopulations. Differences were considered significant when $p<0.05$ as indicated with an asterisks as *$p<0.05$, **$p<0.01$, ***$p<0.001$, and ****$p<0.0001$. Statistical analysis was performed using GraphPad Prism 8.3.1 (San Diego, USA).

RESULTS

CD39 is expressed by $CD8^+$ and $CD4^+$ TIL in different types of cancer

To explore the expression of CD39 on $CD4^+$ T cells, a total of 30 cryopreserved single-cell tumor digests (9 cervical squamous cell carcinoma (CxCa), 10 vulvar squamous cell carcinoma (VSCC), and 11 oropharyngeal squamous cell carcinoma (OPSCC) was stained with a panel of antibodies to phenotype the lineage (CD3, CD4, CD8), central and effector memory type (CCR7, CD45RA), tissue-residency (CD39, CD103), and activation or cytolytic capacity (CD38,

PD-1, HLA-DR, NKG2A, CD161; supplemental table 1). Hierarchical Stochastical Neighbor Embedding (HSNE)[29] analysis revealed 15 subpopulations of T cells, which were present at similar percentages in all three types of cancer (figure 1a, supplemental figure 1). About half of the $CD8^+$ population displayed CD39, often in co-expression with CD103, PD-1, HLA-DR, NKG2A, and CD161, whereas the CD39-negative population rarely expressed PD-1 or CD45RA (figure 1B-D). The $CD4^+$ T cell population tended to comprise more $CD39^+$ cells co-expressing CD38, PD-1, and HLA-DR, while a small percentage also co-expressed CD103 and CD161 (figure 1 B-D, supplemental figure 2A). The percentage of CD39-expressing $CD4^+$ T cells was much higher in tumors (~25%) than in the blood (~1%), suggesting their tumor-specific accumulation (supplemental figure 2B). Analysis of the TIL according to the gating strategy shown in supplemental figure 3A-B showed that the great majority of $CD8^+$ TIL were either double-positive (DP) or double-negative (DN) for CD39 and CD103. Furthermore, there was a small population of single-positive (SP) $CD103^+$ and a rare population of SP $CD39^+$ $CD8^+$ T cells (figure 1D), conform an earlier report.[18] In contrast, the SP $CD39^+$ and the DN populations were most dominant among $CD4^+$ TIL, while the DP population was much smaller and the SP $CD103^+$ populations was rare among $CD4^+$ TIL (figure 1D). The distribution of these 4 subpopulations was similar among all 3 cancer types.

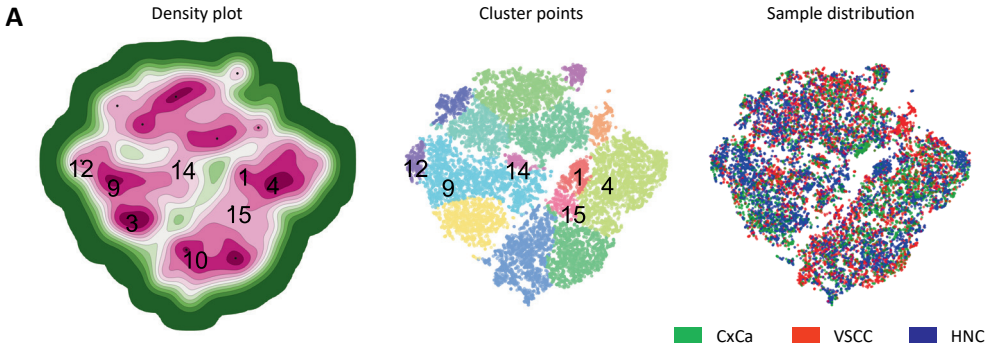

Figure 1. CD39 is expressed by $CD8^+$ and $CD4^+$ TIL in different types of cancer. Cryopreserved single cell tumor digests of patients with CxCa, VSCC and OPSCC were analyzed by 13-parameter flow cytometry analysis. (A) An HSNE density plot (left) and corresponding cluster point plot (middle) and sample distribution plot (right) visualizing the high-dimensional flow cytometry data in two dimensions for the collective immune cells derived from 30 patients (*n*=9 CxCa, *n*=10 VSCC and *n*=11 OPSCC). The identified cell subsets are indicated in the density and cluster point plots by numbers. The contribution of the different tumors to the clustering is depicted in the sample distribution plot by the different colors (CxCa in green, VSCC in red and OPSCC in blue). (B) HSNE dot plots of the immune cells at the single-cell level. Colors represents arcsin150-transformed marker expression as indicated. (C) Minimum Spanning Tree (MST) displaying star plots of the clusters identified by FlowSOM analysis using the cytobank platform. The mean intensities of the clustering channels are depicted by the different colors in the pie chart. The total T cell populations separates into $CD4^+CD39^+$, $CD4^+CD39^-$ and $CD4^+CD39^+CD103^+$ populations (left, in green) and $CD8^+CD39^+CD103+$ and $CD8^+CD39^-CD103^+$ populations (right, purple). (D) Graphs depicting the percentage of $CD39^+CD103^-$, $CD39^+CD103^+$, $CD39^-CD103^-$ and $CD39^-CD103^+$ CD4+ (left) and $CD8^+$ (right) T cells within CxCa (green), VSCC (red) and OPSCC (blue) patients. Patients used in expansion and HPV reactivity assays are depicted by the open circles. **p*<0.05, ***p*<0.01, ****p*<0.001 and *****p*<0.0001.

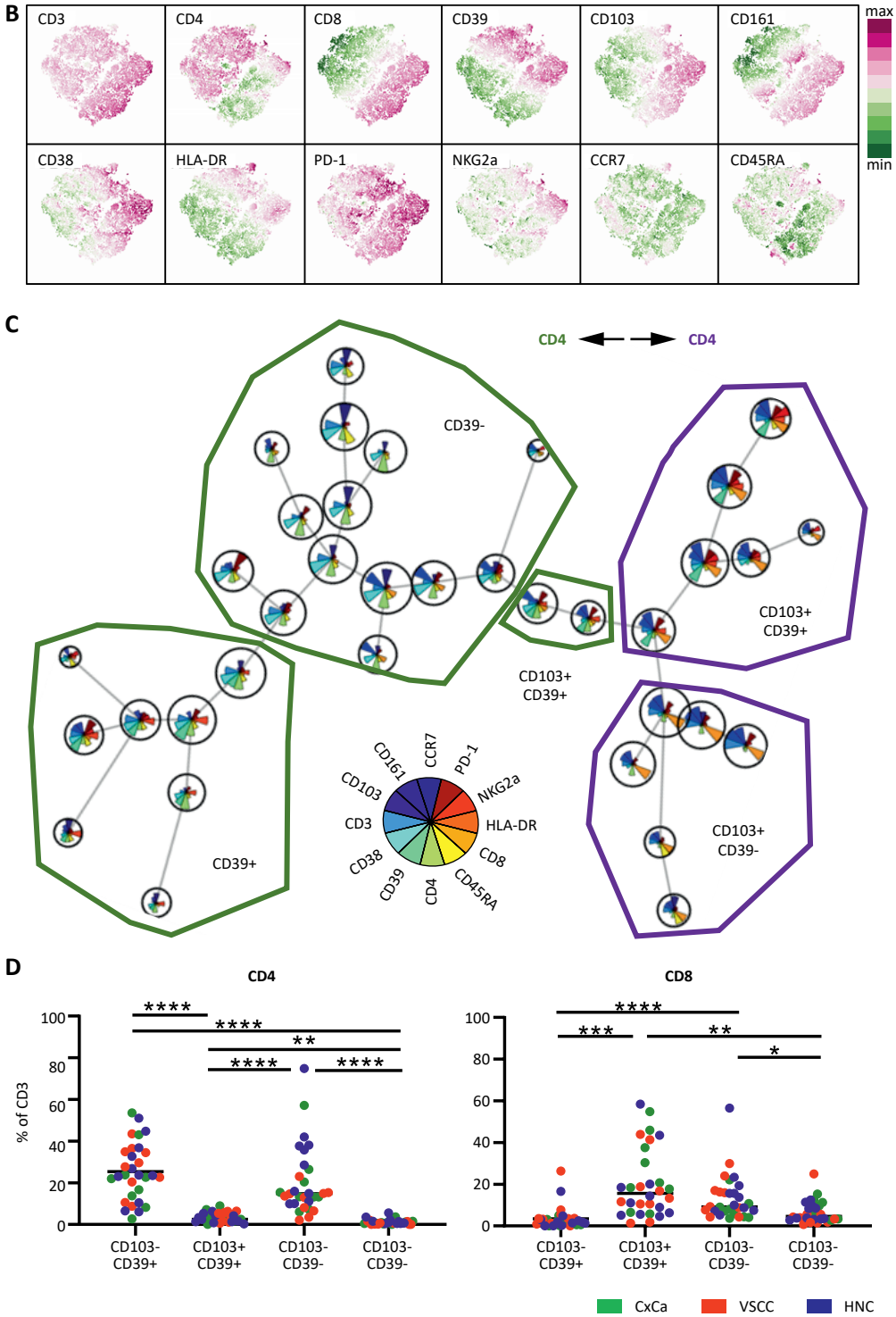

Figure 1. Continued

Intratumoral CD39-positive CD4⁺ and CD8⁺ TIL share markers of activation and tissue-residency

The DP CD4⁺ and CD8⁺ populations exclusively comprised memory T cells, most prominently of an effector memory phenotype (figure 2A-B). While the larger CD4⁺CD39⁺ SP population exhibited a similar phenotype as the DP population, the DN CD4⁺ TIL population was more of a central memory phenotype (figure 2A). In addition, the DP CD4⁺ and CD8⁺ populations comprised the highest percentage of PD-1, HLA-DR, CD38, CD161 and NKG2A (predominantly CD8⁺ TIL) expressing cells (figure 2C-D supplemental figure 4A-B) and the highest expression levels of PD-1 and HLA-DR (supplemental figure 4C-D) emphasizing that they were highly activated. The percentage of HLA-DR-expressing cells was also higher in the SP CD39⁺ population when compared to the CD4⁺ and CD8⁺ DN or SP CD103⁺ TIL populations (figure 2C-D), suggesting that also the SP CD39⁺ T cells may have been locally activated. Remarkably, a high percentage of CD4⁺ T cells expressing NKG2A⁺ was found in two of nine VSCC patients and none of the CxCa and OPSCC patients. Apparently, this is a VSCC-specific feature as a reanalysis of nine VSCC samples from a previous study[27] and seven additional OPSCC TILs revealed that high percentages of NKG2A⁺ CD4⁺ TILs were found in five of 18 VSCC, but not in any of the 27 OPSCC or CxCa (supplemental figure 4E).

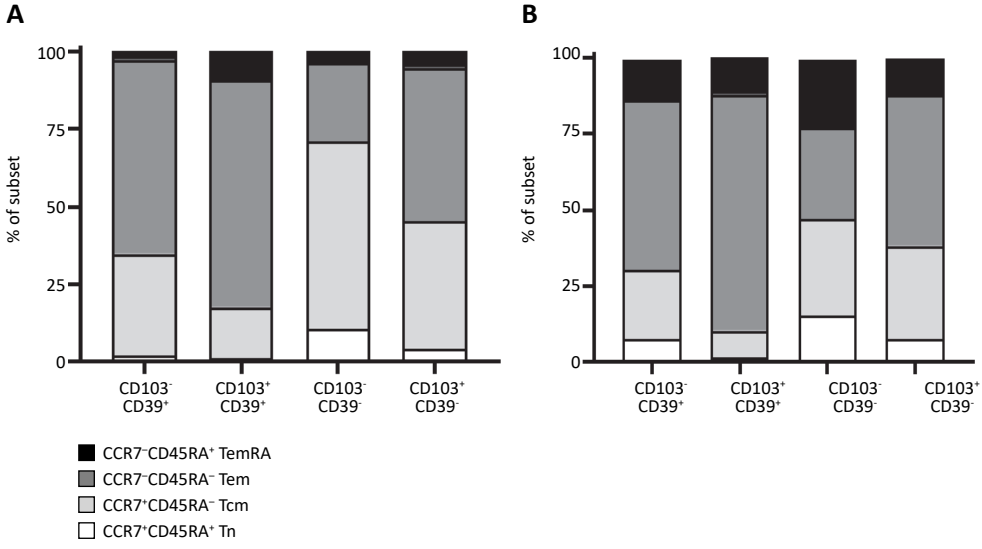

Figure 2. Intratumoral CD39⁺ CD4⁺ and CD8⁺ TIL are highly activated. Cryopreserved single cell tumor digests of patients with CxCa, VSCC and OPSCC were analyzed by 13-parameter flow cytometry analysis. (A, B) Stacked bar graphs showing the subdivision of the CD39⁺CD103⁻, CD39⁺CD103⁺, CD39⁻CD103⁻ and CD39⁻CD103⁺ CD4⁺ (A) and CD8⁺ (B) T cells into naïve T cells (Tn, white, CCR7⁺CD45RA⁺), central memory T cells (Tcm, light grey, CCR7+CD45RA⁻), effector memory T cells (Tem, dark grey, CCR7⁻CD45RA⁻) and CD45RA⁺ effector memory T cells (Temra, black, CCR7−CD45RA⁺ C, D) Graphs depicting the percentage of PD-1 (top) and HLA-DR (bottom) within CD39⁺CD103⁻, CD39⁺CD103⁺, CD39⁻CD103⁻ and CD39⁻CD103⁺ CD4⁺ (C) and CD8⁺ (D) T cells within CxCa (green, *n*=9), VSCC (red, *n*=10) and OPSCC (blue, *n*=11) patients. Patients used in expansion and HPV reactivity assays are depicted by the open circles. **p*<0.05, ***p*<0.01, ****p*<0.001 and *****p*<0.0001.

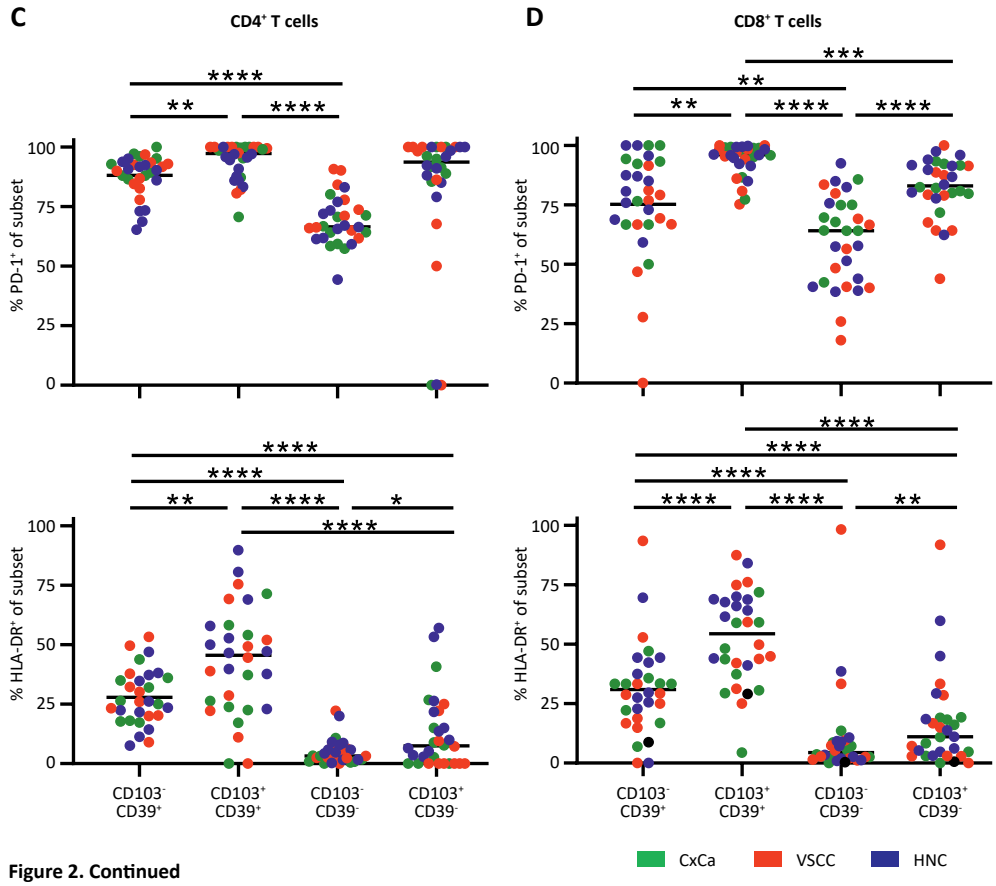

Figure 2. Continued

CD4⁺ T cells expressing CD39 have mainly been classified as regulatory T cells (Tregs) based on the co-expression of Foxp3 and CTLA-4 or by the large production of IL-10.[37] However, CD4⁺CD39⁺ effector memory T cells secreting IFNγ and IL-17 have been detected in the blood of patients with renal allograft rejection[38], indicating that CD39 expression is not a marker of suppressive T cells *per se*. To address if the CD4⁺CD39⁺ TILs were Tregs or activated effector T cells, we analyzed the CD4⁺CD39⁺ T cells both in PBMC and in 4 single cell tumor digests (*n*=2 VSCC and *n*=2 CxCa) by flow cytometry using our previously described essential Treg marker set.[28] Analysis showed that on average 78.8% (95%CI 69.4–94.9; *n*=4)) of the CD4⁺CD39⁺ TILs did not fall into the category of CD25⁺Foxp3⁺ Tregs (supplemental figure 4F). A similar percentage of CD4⁺CD39⁺ T cells expressing CD25 and Foxp3 was also found in the blood (supplemental figure 4F), but here the CD39⁺ T cell population was much smaller (supplemental figure 2B). Furthermore, a larger proportion of the CD4⁺CD39⁺ TILs exhibited an CD25⁺Foxp3⁻ activated non-Treg phenotype, illustrating that the CD4⁺CD39⁺ T cells in tumors or tissues - which can't be excluded as we had no healthy tissue to compare with - have a more activated profile (supplemental figure 4F). In addition, we also performed single-

cell RNA sequencing analysis on magnetic bead-sorted $CD3^+$ T cells from 13 OPSCC samples, yielding data for 20.199 T cells. Unsupervised clustering using the Leiden algorithm[34] as implemented in the scanpy package[31], resulted in 23 different $CD4^+$ and $CD8^+$ TIL clusters (figure 3A). Within these 23 clusters, three populations of CD39 (*ENTPD1*)-expressing cells existed, being $CD4^+$ T cells, $CD8^+$ T cells and $CD4^+Foxp3^+$ Treg cells. The $CD8^+CD39^+$ TIL cluster also expressed the tissue-residency markers *ALOX5AP*, *ITGAE* (CD103), and *ITGA1* (CD49a)[39], as well as genes associated with exhaustion/activation (*PDCD1* (PD-1), *LAG-3, CXCL13*) and with their function to control tumor cell growth (*IFNγ, GNLY* (granulysin), *GZMB* (granzyme B), *PRF1* (perforin)).[40, 41] One of the two identified $CD4^+CD39^+$ TIL clusters clearly expressed *Foxp3* and *IL-2RA* (CD25), marking them as Tregs (figure 3). The second $CD4^+CD39^+$ TIL cluster did not express these Treg markers, but showed a gene expression profile more closely related to the $CD8^+CD39^+$ TILs, with high expression of *ALOX5AP, CXCL13* and *PDCD1*, as well as with substantial expression of *LAG-3*, *IFNγ*, *GNLY* and *GZMB* (figure 3B), indicating that they are more likely to represent pro-inflammatory effector cells and, as such, may contain tumor-reactive T cells. The $CD4^+CD39^+$ and $CD8^+CD39^+$ TIL also expressed several genes associated with exhaustion/co-inhibition as well as a substantial number of genes associated with activation/co-stimulation. The expression of genes associated with activation was more pronounced in $CD4^+CD39^+$ TIL, and included *CD40LG*, suggesting that this $CD39^+CD4^+$ T cell population displayed a more activated rather than exhausted T cell profile (supplemental figure 5). We further illustrate the similarity between the tissue resident memory T cell (Trm) and pro-inflammatory effector T cell profile for $CD8^+CD39^+$ and $CD4^+CD39^+$ T cells by pairwise comparisons of differentially expressed genes (DEG) between these T cells and the cluster of $CD4^+CD39^+$ Tregs. This showed an overlap in 15 of the 50 most significant DEGs (figure 3C).

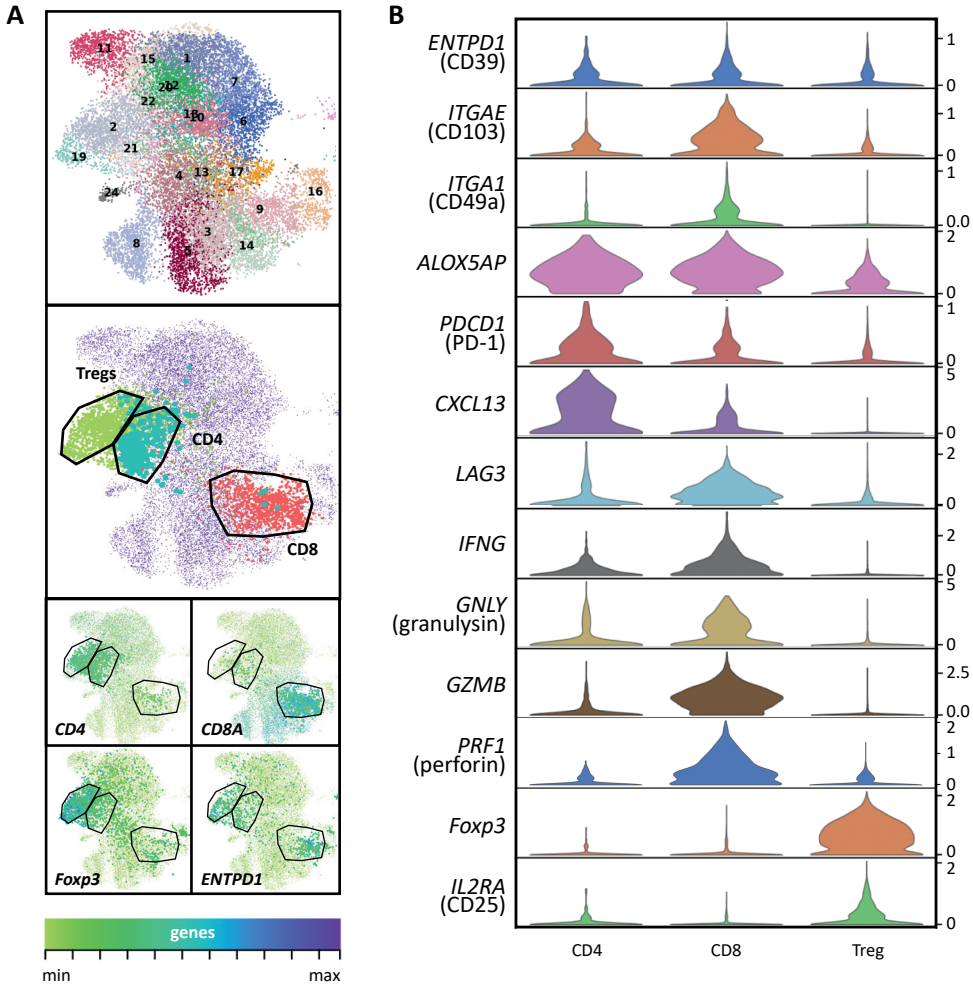

Figure 3. Intratumoral CD39⁺ CD4⁺ and CD8⁺ TIL share markers of activation and tissue-residency. Single-cell RNA sequencing analysis was performed on magnetic-bead sorted 20,199 $CD3^+$ T cells from 13 OPSCC samples. (A) 2-dimensional UMAP plots visualizing the 23 clusters identified using the Leiden algorithm (top UMAP), and three $CD39^+$ populations comprising $CD4^+$ T cells, $CD8^+$ T cells and $CD4^+Foxp3^+$ regulatory T cells (Tregs, middle and bottom UMAP). Expression level of *CD4*, *CD8A*, *Foxp3* and *ENTPD1* (CD39) at the single cell level is depicted in color code. (B) Stacked violin plot depicting expression levels of *ENTPD1* (CD39), *ITGAE* (CD103), *ITGA1* (CD49a), *ALOX5AP*, *PDCD1*, *CXCL13*, *LAG3*, *IFNG*, *GNLY* (granulysin), *GZMB* (granzyme B), *PRF1* (perforin), *Foxp3* and *IL2RA* (CD25) for the indicated three populations. (C) Graph displaying the top 50 significantly ($p<9.2x10e-20$) differentially expressed genes (DEG) between $CD4^+CD39^+$ (left) and $CD8^+CD39^+$ (right) and $CD39^+$ Tregs. Values depicted are log^2 fold change (log^2FC) values. Overlap in DEG expression in the pairwise comparison between $CD4^+CD39^+$ and $CD8^+CD39^+$ and Tregs is depicted by the green circles (up) and red circles (down) in $CD4^+CD39^+$ and $CD8^+CD39^+$ cells compared to Tregs).

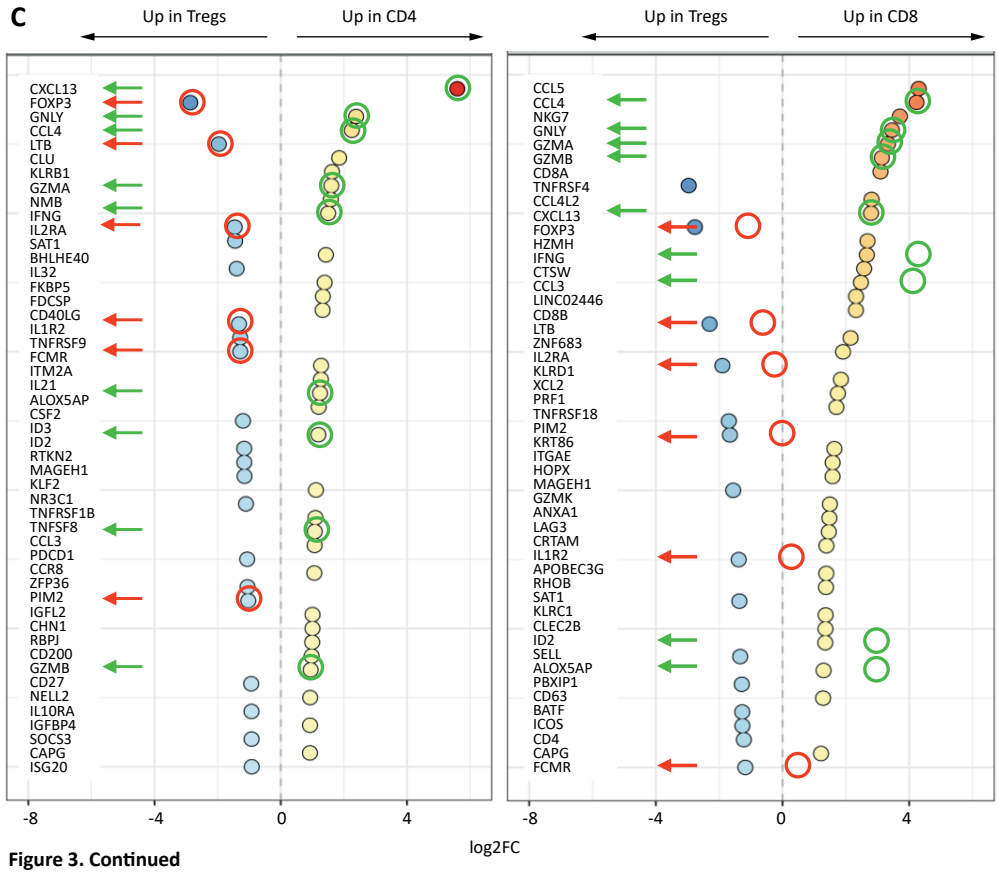

Figure 3. Continued

CD39⁺ TIL are readily expanded in vitro and are the main population responding to tumor antigens

Taking advantage from the fact that a number of these tumors were caused by high-risk human papillomavirus and as a consequence express the highly immunogenic tumor-specific antigens E6 and E7[26, 42], we sorted cryopreserved single-cell tumor digests from seven HPV-associated tumors (*n*=2 CxCa, *n*=3 OPSCC, *n*=2 VSCC) into $CD4^+CD39^-$, $CD4^+CD39^+$, $CD8^+CD39^-CD103^+$ and $CD8^+CD39^+CD103^+$ TIL populations (supplemental figure 6) yielding highly pure populations of cells (figure 4A-B). In all cases sufficient cells were obtained to allow for two rounds of expansion using CD3/CD28 beads and a mix of TCG-F, IL-7, IL-15 and IL-21. Cell fractions obtained at cell counts of less than 1000 cells were expanded to a few millions and then to several million cells (supplemental table 2), delivering enough cells of each population to assess their specificity (figure 4C-D). Phenotypic analysis of the expanded T cell populations revealed that the expression of the cell surface markers CD39 and CD103 may change after *in vitro* culture outside the context of the tumor microenvironment (supplemental figure 7A-B), indicating that cell sorting for tumor-reactive T cells has to be performed directly on single tumor cell digests. No expansion of $CD39^+Foxp3^+$ Tregs was observed (supplemental figure 7C-D).

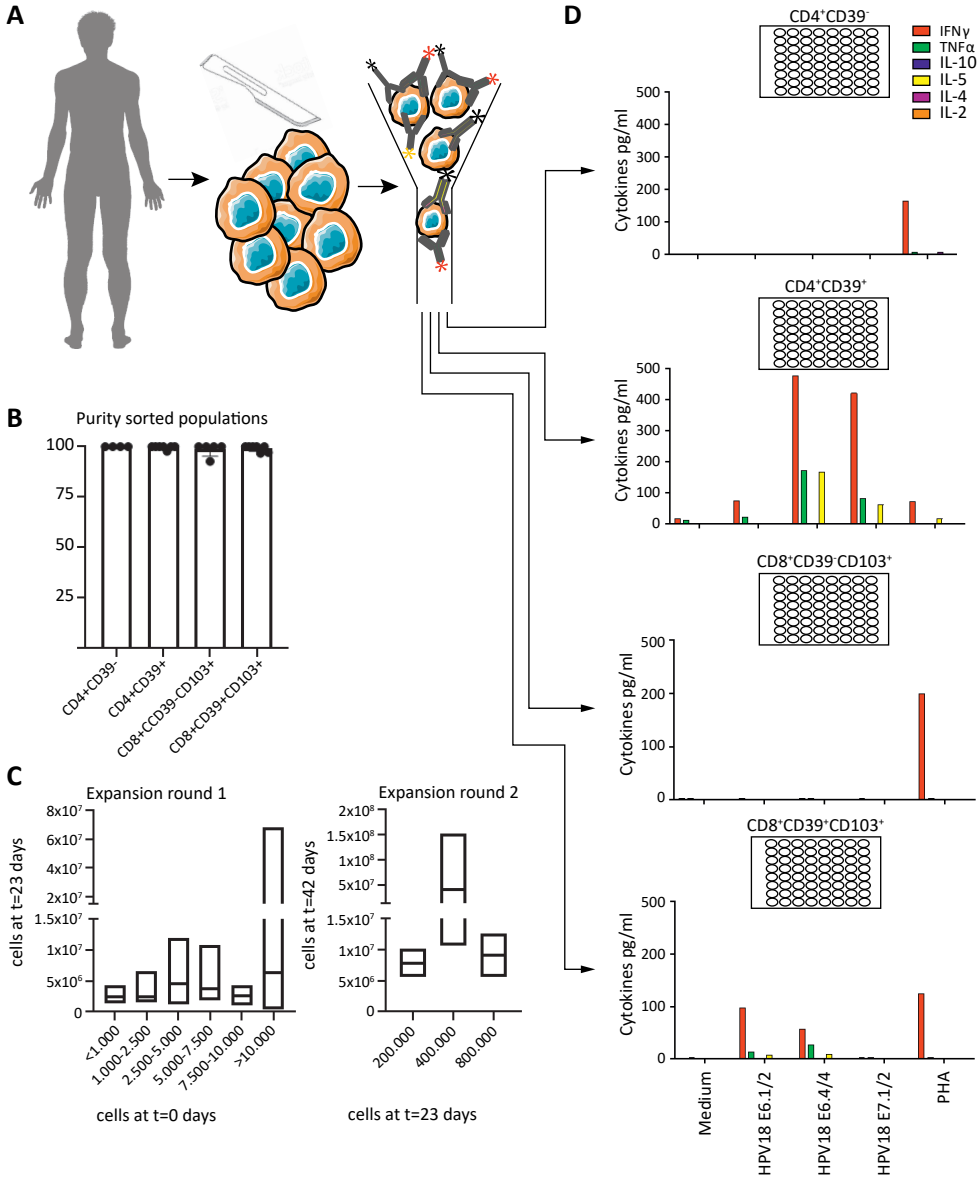

Figure 4. Schematic workflow of CD39⁺ T cell sorting, expansion and functional testing. (A) HPV-induced CxCa, VSCC, or OPSCC tumors freshly obtained from surgery, were cut into small pieces, digested through enzymatic dissociation into single cells, and stored in the vapor phase of liquid nitrogen and were then thawed and stained with fluorochrome-labeled antibodies directed against CD4, CD8, CD39, and CD103. Next, the cells were sorted using a FACS ARIAIII into $CD4^+CD39^-$, $CD4^+CD39^+$, $CD8^+CD39^-CD103^+$ and $CD8^+CD39^+CD103^+$ populations and subsequently expanded. (B) Graph showing the purity of the sorted populations (*n*=23). (C) Graph displaying the number of cells after expansion round 1 (day 23, left) and expansion round 2 (day 42, right). Populations are grouped based on the depicted numbers obtained at the start of expansion round 1 (day 0, left) or round 2 (and day 23, right). (D) Graphs displaying the cytokine production of $CD4^+CD39^-$, $CD4^+CD39^+$, $CD8^+CD39^-CD103^+$ and $CD8^+CD39^+CD103^+$ cells in response to HPV18 E6 peptide pools (pool 1+2 and 3+4) and E7 peptide pools (pool 1+2)-loaded autologous monocytes for a representative VSCC patient. Cytokines are measured by Th1/Th2 cytometric bead array (CBA) and depicted in pg/ml.

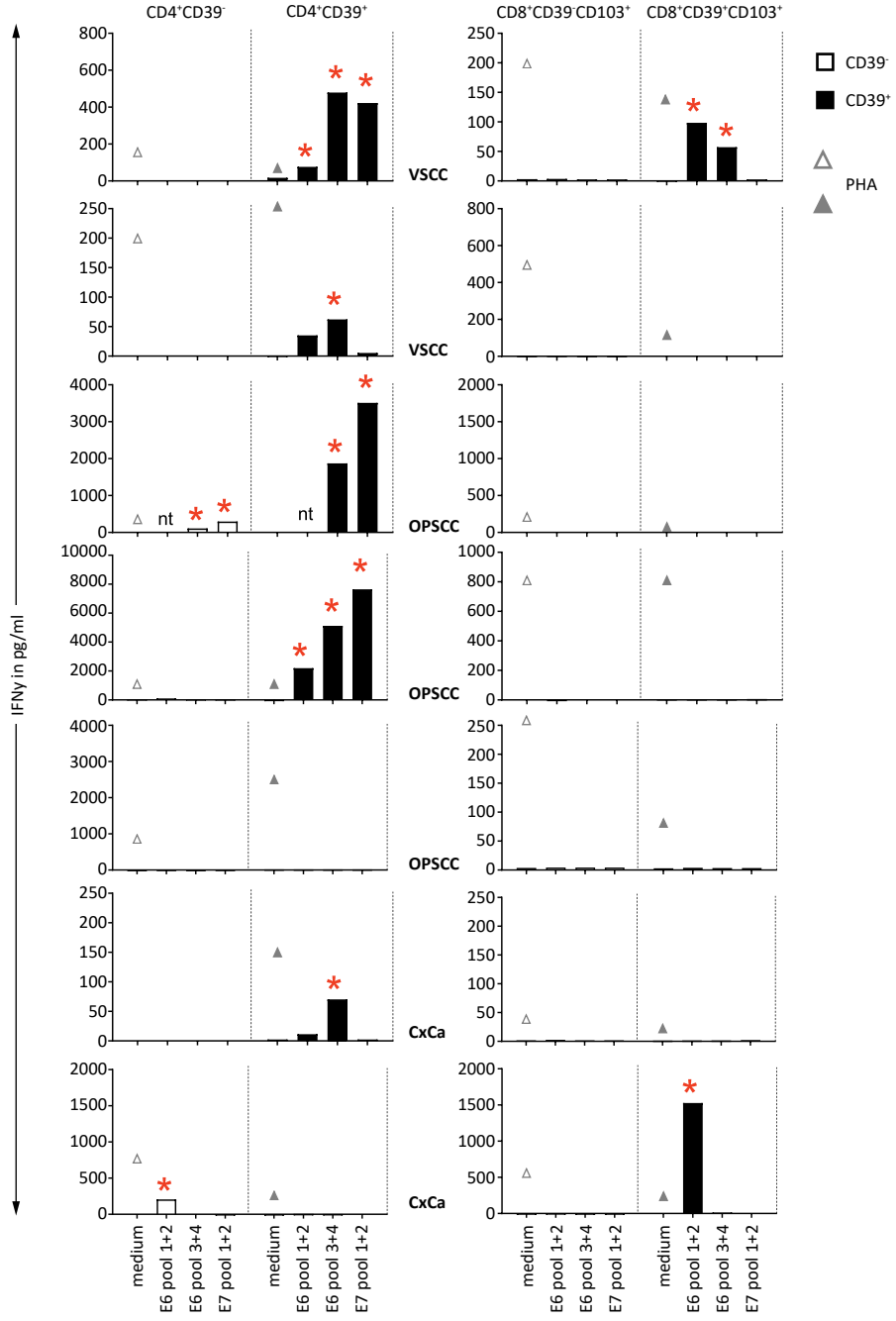

Figure 5. Predominant detection of HPV-specific reactivity amongst CD4$^+$CD39$^+$ and CD8$^+$CD39$^+$CD103$^+$ TIL. Graphs displaying the IFNγ production of CD4$^+$CD39$^-$ and CD4$^+$CD39$^+$ TIL (left) and CD8$^+$CD39$^-$CD103$^+$ and CD8$^+$CD39$^+$CD103$^+$ TIL in response to medium (control) or the HPV16 or HPV18 E6 peptide pools (pool 1+2 and 3+4) and E7 peptide pools (pool 1+2)-loaded autologous monocytes for seven HPV-associated SCC (*n*=2 VSCC, *n*=3 OPSCC, *n*=2 CxCa from top to bottom). IFN-γ production in response to PHA, which served as a positive control, is depicted with the grey triangles. Positive cytokine production, which is defined as at least twice above that of the medium stimulated cells and above the assay cut-off, is indicated by the red asterisk.

In 6 of the 7 patients a response to E6 and/or E7 was detected (figure 5). Two of the patients displayed a tumor-specific $CD8^+$ T cell response, in both cases only detected in the $CD8^+CD39^+CD103^+$ fraction. Six of the patients showed $CD4^+$ T cell reactivity against E6 and/or E7 by specifically producing IFNγ. In five cases the response was measured in the $CD39^+$ sorted cell fraction of $CD4^+$ T cells. In two cases a weak response was found in the CD39-negative fraction, one of which was also detected at much higher levels in the $CD39^+$ cell population (figure 5). In all cases, the production of the type-1 cytokine IFNγ dominated the response, but occasionally also low amounts of the type-2 cytokines IL-10 and IL-5 were measured (supplemental figure 8). These data clearly show that tumor-specific antigen reactivity was almost exclusively detected among $CD39^+$ TIL.

DISCUSSION

In this study, we show that tumors may contain two populations of $CD4^+$ T cells expressing CD39. While one of these populations displays markers of Tregs, the other exhibits an activated tissue-resident non-regulatory profile similar to that of the $CD39^+CD103^+CD8^+$ TIL population and this $CD4^+CD39^+$ T cell fraction can be readily expanded and is enriched with tumor-specific T cells.

The search for an optimal marker to dissect bystander activated T cells that co-infiltrate tumor tissue from tumor-reactive T cells, led to the realization that TILs expressing the tissue-resident marker CD103 [43] and the chronic local antigen stimulation marker CD39[11] may be enriched for tumor-reactive T cells. Indeed, $CD8^+CD39^+CD103^+$ TIL from melanoma[18], colorectal cancer[20], VSCC and CxCa (this study), were highly enriched for tumor-reactive T cells. Importantly, while the SP $CD8^+CD39^+$ TIL are rare and the DP CD8+ TIL are frequently detected by flow cytometry, the opposite holds true for $CD4^+$ TIL. The DP tissue-resident TILs among both $CD4^+$ and $CD8^+$ TIL most likely are locally stimulated highly active T cells, based on the highest expression of PD-1, HLA-DR, and CD38. However, we show that also the SP $CD39^+$ T cells display such an activated profile, hence CD39 as a marker for local chronic activation may by itself identify both $CD8^+$ and $CD4^+$ tumor-reactive T cells when markers for Tregs are also applied.

This notion is corroborated by our single cell RNA analyses of the three cell clusters of T cells expressing CD39. Not only did the $CD4^+CD39^+$ non-Treg cluster express genes associated with a functional antitumor response but it also expressed genes associated with cell retention in the tumor (e.g. *ITGAE, ITGA1*) or associated with tumor-residency (e.g. *ALOX5AP, CXCL13*). Moreover, in comparison to the $CD39^+$ Tregs, the $CD4^+CD39^+$ effector T cell population had 15 out of the top 50 differentially expressed genes in common with the $CD8^+CD39^+$ tumor-resident population. Finally, although the expression of CD39 often is associated with T

cells displaying an exhausted phenotype, the $CD4^+CD39^+$ non-Treg cluster also displayed a substantial number of activation/costimulatory genes arguing against exhaustion and fitting with the fact that they readily expanded and responded to cognate antigen *in vitro.*

It is well established that when naïve $CD4^+$ T cells encounter their cognate antigen presented by dendritic cells they become activated and can migrate to tumors. Less is known about the fate of these cells in the TME, in particular how their activation is maintained. The expression of CD39 and CD103 in combination with other markers such as CD38, HLA-DR, and PD-1 on these $CD4^+$ T cells sheds some light on this mechanism as it implies that $CD4^+$ T cells are retained in the tumor to locally receive their stimulus. Indeed, chronic TCR stimulation, a process that must frequently occur in the TME, and the presence of certain cytokines (e.g. TGFβ, IL-6, IL-27) drives the expression of CD39 on T cells.[18, 44] The signals for cell retention in the TME are most likely mediated by local macrophages[45] but potentially also via interaction with MHC class II positive tumor cells.[46, 47] CD39, which is an ectonucleotidase that regulates extracellular ATP/adenosine levels, potentially also plays a role in the retention of these cells in the TME. Extracellular ATP allows trafficking of immune cells and this is blocked by adenosine[48-50], effectively keeping the T cells in the tumor. CD39 may also function to counterbalance the ongoing immune response in tumors by suppressing local T cell proliferation and effector function[50, 51], perhaps in order to prevent immune pathology.

The isolation and expansion of TIL enriched for tumor-reactive T cells may aid the identification of new tumor antigens and improve the development of clinically oriented applications such as the adoptive transfer of either TCR transgenic T cells or bulk T-cell cultures, which have been shown to be effective in a number of cancers.[46, 52-58] The isolated and expanded DP $CD8^+$ TIL in our study responded to the E6 and E7 tumor-specific antigens in two of seven cases, while such a response was observed in 5 of the 7 $CD4^+CD39^+$ TIL cultures. The low response rate to E6 and E7 by $CD8^+$ T cells is in line with earlier observations showing the presence of much higher frequencies of E6/E7-specific $CD4^+$ TILs than E6/E7-specific $CD8^+$ TILs in these types of tumors[26] and observations that neoantigens are likely to be targeted by $CD8^+$ T cells.[59] In addition, only limited amounts of single-cell tumor digest material, stored in liquid nitrogen, was available which further restricted the chance to isolate the scarcer E6/E7-specific $CD8^+$ T cells. Clinical oriented application of isolated $CD39^+$ T cells, therefore, may benefit from more and freshly isolated single-cell digests. The fact that also regulatory $CD4^+$ T cells express CD39[37] provides the theoretical problem that Tregs are co-amplified and/or may prevent the outgrowth of the $CD39^+$ tumor-reactive effector cells. Post-expansion analyses of the $CD4^+CD39^+$ T cell cultures showed that this was not the case, with less than 1.8% of $CD25^+Foxp3^+$ Tregs being present in the cultures after expansion.

In conclusion, we propose that primed tumor-specific T cells migrating to the tumor receive a series of antigenic stimuli following cognate interactions with tumor cells or local APC, with

as a result that CD39 is upregulated on both $CD8^+$ and $CD4^+$ TIL. The identification of CD39 as a marker for both $CD4^+$ and $CD8^+$ tumor-reactive T cells will be highly useful with respect to studies on the susceptibility or resistance of several immunotherapeutic approaches for cancer, including checkpoint blockade, ACT and therapeutic vaccines. Last but not least, CD39 blockade - in a setting where human T cells were the only cells expressing CD39 - stimulated their trafficking, proliferation and IFN-γ production.[50] In combination with our data, this drives the expectation that tumors with a high $CD39^+$ T cell count are the best to respond to CD39 blockade therapy.

ACKNOWLEDGEMENTS

We gratefully thank all the patients and healthy individuals who participated in this study. Furthermore, we thank Sandra van der Broek-Veldstra and Lena van Doorn for including the patients in the CIRCLE Study.

REFERENCES

1. Fridman, W.H., et al., *The immune contexture in human tumours: impact on clinical outcome.* Nat Rev Cancer, 2012. 12(4): p. 298-306.
2. Shankaran, V., et al., *IFNgamma and lymphocytes prevent primary tumour development and shape tumour immunogenicity.* Nature, 2001. 410(6832): p. 1107-11.
3. Galon, J. and D. Bruni, *Approaches to treat immune hot, altered and cold tumours with combination immunotherapies.* Nat Rev Drug Discov, 2019. 18(3): p. 197-218.
4. Hung, K., et al., *The central role of CD4(+) T cells in the antitumor immune response.* J Exp Med, 1998. 188(12): p. 2357-68.
5. van den Broeke, L.T., et al., *Dendritic cell-induced activation of adaptive and innate antitumor immunity.* J Immunol, 2003. 171(11): p. 5842-52.
6. Doorduijn, E.M., et al., *CD4(+) T Cell and NK Cell Interplay Key to Regression of MHC Class I(low) Tumors upon TLR7/8 Agonist Therapy.* Cancer Immunol Res, 2017. 5(8): p. 642-653.
7. Kang, T.W., et al., *Senescence surveillance of pre-malignant hepatocytes limits liver cancer development.* Nature, 2011. 479(7374): p. 547-51.
8. Bos, R. and L.A. Sherman, *CD4+ T-cell help in the tumor milieu is required for recruitment and cytolytic function of CD8+ T lymphocytes.* Cancer Res, 2010. 70(21): p. 8368-77.
9. Klebanoff, C.A., L. Gattinoni, and N.P. Restifo, *CD8+ T-cell memory in tumor immunology and immunotherapy.* Immunol Rev, 2006. 211: p. 214-24.
10. Cheon, H., E.C. Borden, and G.R. Stark, *Interferons and their stimulated genes in the tumor microenvironment.* Semin Oncol, 2014. 41(2): p. 156-73.
11. Simoni, Y., et al., *Bystander CD8(+) T cells are abundant and phenotypically distinct in human tumour infiltrates.* Nature, 2018. 557(7706): p. 575-579.
12. Scheper, W., et al., *Low and variable tumor reactivity of the intratumoral TCR repertoire in human cancers.* Nat Med, 2019. 25(1): p. 89-94.
13. Ye, Q., et al., *CD137 accurately identifies and enriches for naturally occurring tumor-reactive T cells in tumor.* Clin Cancer Res, 2014. 20(1): p. 44-55.
14. Parkhurst, M., et al., *Isolation of T-Cell Receptors Specifically Reactive with Mutated Tumor-Associated Antigens from Tumor-Infiltrating Lymphocytes Based on CD137 Expression.* Clin Cancer Res, 2017. 23(10): p. 2491-2505.
15. Choi, B.K., et al., *4-1BB-based isolation and expansion of CD8+ T cells specific for self-tumor and non-self-tumor antigens for adoptive T-cell therapy.* J Immunother, 2014. 37(4): p. 225-36.
16. Fernandez-Poma, S.M., et al., *Expansion of Tumor-Infiltrating CD8(+) T cells Expressing PD-1 Improves the Efficacy of Adoptive T-cell Therapy.* Cancer Res, 2017. 77(13): p. 3672-3684.
17. Gros, A., et al., *PD-1 identifies the patient-specific CD8(+) tumor-reactive repertoire infiltrating human tumors.* J Clin Invest, 2014. 124(5): p. 2246-59.
18. Duhen, T., et al., *Co-expression of CD39 and CD103 identifies tumor-reactive CD8 T cells in human solid tumors.* Nat Commun, 2018. 9(1): p. 2724.

19. Martinez-Usatorre, A., et al., *Enhanced Phenotype Definition for Precision Isolation of Precursor Exhausted Tumor-Infiltrating CD8 T Cells.* Front Immunol, 2020. 11: p. 340.
20. van den Bulk, J., et al., *Neoantigen-specific immunity in low mutation burden colorectal cancers of the consensus molecular subtype 4.* Genome Med, 2019. 11(1): p. 87.
21. Levitsky, H.I., et al., *In vivo priming of two distinct antitumor effector populations: the role of MHC class I expression.* J Exp Med, 1994. 179(4): p. 1215-24.
22. Quezada, S.A., et al., *Tumor-reactive CD4(+) T cells develop cytotoxic activity and eradicate large established melanoma after transfer into lymphopenic hosts.* J Exp Med, 2010. 207(3): p. 637-50.
23. Tran, E., et al., *Cancer immunotherapy based on mutation-specific CD4+ T cells in a patient with epithelial cancer.* Science, 2014. 344(6184): p. 641-5.
24. Hunder, N.N., et al., *Treatment of metastatic melanoma with autologous CD4+ T cells against NY-ESO-1.* N Engl J Med, 2008. 358(25): p. 2698-703.
25. Kansas, G.S., G.S. Wood, and T.F. Tedder, *Expression, distribution, and biochemistry of human CD39. Role in activation-associated homotypic adhesion of lymphocytes.* J Immunol, 1991. 146(7): p. 2235-44.
26. Welters, M.J.P., et al., *Intratumoral HPV16-Specific T Cells Constitute a Type I-Oriented Tumor Microenvironment to Improve Survival in HPV16-Driven Oropharyngeal Cancer.* Clin Cancer Res, 2018. 24(3): p. 634-647.
27. Kortekaas, K.E., et al., *High numbers of activated helper T cells are associated with better clinical outcome in early stage vulvar cancer, irrespective of HPV or p53 status.* J Immunother Cancer, 2019. 7(1): p. 236.
28. Santegoets, S.J., et al., *Monitoring regulatory T cells in clinical samples: consensus on an essential marker set and gating strategy for regulatory T cell analysis by flow cytometry.* Cancer Immunol Immunother, 2015. 64(10): p. 1271-86.
29. van Unen, V., et al., *Visual analysis of mass cytometry data by hierarchical stochastic neighbour embedding reveals rare cell types.* Nat Commun, 2017. 8(1): p. 1740.
30. Zheng, G.X., et al., *Massively parallel digital transcriptional profiling of single cells.* Nat Commun, 2017. 8: p. 14049.
31. Wolf, F.A., P. Angerer, and F.J. Theis, *SCANPY: large-scale single-cell gene expression data analysis.* Genome Biol, 2018. 19(1): p. 15.
32. Luecken, M.D. and F.J. Theis, *Current best practices in single-cell RNA-seq analysis: a tutorial.* Mol Syst Biol, 2019. 15(6): p. e8746.
33. Wolock, S.L., R. Lopez, and A.M. Klein, *Scrublet: Computational Identification of Cell Doublets in Single-Cell Transcriptomic Data.* Cell Syst, 2019. 8(4): p. 281-291.e9.
34. Traag, V.A., L. Waltman, and N.J. van Eck, *From Louvain to Leiden: guaranteeing well-connected communities.* Sci Rep, 2019. 9(1): p. 5233.
35. McInnes, L. and J. Healy, *UMAP: uniform manifold approximation and projection for dimension reduction. .* 2018.

36. Robinson, M.D., D.J. McCarthy, and G.K. Smyth, *edgeR: a Bioconductor package for differential expression analysis of digital gene expression data.* Bioinformatics, 2010. 26(1): p. 139-40.
37. Allard, B., et al., *The ectonucleotidases CD39 and CD73: Novel checkpoint inhibitor targets.* Immunol Rev, 2017. 276(1): p. 121-144.
38. Dwyer, K.M., et al., *Expression of CD39 by human peripheral blood CD4+ CD25+ T cells denotes a regulatory memory phenotype.* Am J Transplant, 2010. 10(11): p. 2410-20.
39. Kumar, B.V., et al., *Human Tissue-Resident Memory T Cells Are Defined by Core Transcriptional and Functional Signatures in Lymphoid and Mucosal Sites.* Cell Rep, 2017. 20(12): p. 2921-2934.
40. Li, H., et al., *Dysfunctional CD8 T Cells Form a Proliferative, Dynamically Regulated Compartment within Human Melanoma.* Cell, 2019. 176(4): p. 775-789.e18.
41. Guo, X., et al., *Global characterization of T cells in non-small-cell lung cancer by single-cell sequencing.* Nat Med, 2018. 24(7): p. 978-985.
42. Piersma, S.J., et al., *Human papilloma virus specific T cells infiltrating cervical cancer and draining lymph nodes show remarkably frequent use of HLA-DQ and -DP as a restriction element.* Int J Cancer, 2008. 122(3): p. 486-94.
43. Djenidi, F., et al., *CD8+CD103+ tumor-infiltrating lymphocytes are tumor-specific tissue-resident memory T cells and a prognostic factor for survival in lung cancer patients.* J Immunol, 2015. 194(7): p. 3475-86.
44. Canale, F.P., et al., *CD39 Expression Defines Cell Exhaustion in Tumor-Infiltrating CD8(+) T Cells.* Cancer Res, 2018. 78(1): p. 115-128.
45. Haabeth, O.A., et al., *How Do CD4(+) T Cells Detect and Eliminate Tumor Cells That Either Lack or Express MHC Class II Molecules?* Front Immunol, 2014. 5: p. 174.
46. Linnemann, C., et al., *High-throughput epitope discovery reveals frequent recognition of neo-antigens by CD4+ T cells in human melanoma.* Nat Med, 2015. 21(1): p. 81-5.
47. Cioni, B., et al., *HLA class II expression on tumor cells and low numbers of tumor-associated macrophages predict clinical outcome in oropharyngeal cancer.* Head Neck, 2019. 41(2): p. 463-478.
48. Mahnke, K., et al., *Down-Regulation of CD62L Shedding in T Cells by CD39(+) Regulatory T Cells Leads to Defective Sensitization in Contact Hypersensitivity Reactions.* J Invest Dermatol, 2017. 137(1): p. 106-114.
49. Adamiak, M., et al., *The Inhibition of CD39 and CD73 Cell Surface Ectonucleotidases by Small Molecular Inhibitors Enhances the Mobilization of Bone Marrow Residing Stem Cells by Decreasing the Extracellular Level of Adenosine.* Stem Cell Rev Rep, 2019. 15(6): p. 892-899.
50. Li, X.Y., et al., *Targeting CD39 in Cancer Reveals an Extracellular ATP- and Inflammasome-Driven Tumor Immunity.* Cancer Discov, 2019. 9(12): p. 1754-1773.
51. Noble, A., et al., *IL-12 and IL-4 activate a CD39-dependent intrinsic peripheral tolerance mechanism in CD8(+) T cells.* Eur J Immunol, 2016. 46(6): p. 1438-48.
52. Doran, S.L., et al., *T-Cell Receptor Gene Therapy for Human Papillomavirus-Associated Epithelial Cancers: A First-in-Human, Phase I/II Study.* J Clin Oncol, 2019. 37(30): p. 2759-2768.

53. Verdegaal, E.M., et al., *Neoantigen landscape dynamics during human melanoma-T cell interactions.* Nature, 2016. 536(7614): p. 91-5.
54. Ramachandran, I., et al., *Systemic and local immunity following adoptive transfer of NY-ESO-1 SPEAR T cells in synovial sarcoma.* J Immunother Cancer, 2019. 7(1): p. 276.
55. Chapuis, A.G., et al., *Regression of metastatic Merkel cell carcinoma following transfer of polyomavirus-specific T cells and therapies capable of re-inducing HLA class-I.* Cancer Immunol Res, 2014. 2(1): p. 27-36.
56. Morgan, R.A., et al., *Cancer regression in patients after transfer of genetically engineered lymphocytes.* Science, 2006. 314(5796): p. 126-9.
57. Stevanovic, S., et al., *A Phase II Study of Tumor-infiltrating Lymphocyte Therapy for Human Papillomavirus-associated Epithelial Cancers.* Clin Cancer Res, 2019. 25(5): p. 1486-1493.
58. Verdegaal, E., et al., *Low-dose interferon-alpha preconditioning and adoptive cell therapy in patients with metastatic melanoma refractory to standard (immune) therapies: a phase I/II study.* J Immunother Cancer, 2020. 8(1).
59. Yang, W., et al., *Immunogenic neoantigens derived from gene fusions stimulate T cell responses.* Nat Med, 2019. 25(5): p. 767-775.

SUPPLEMENTAL MATERIALS

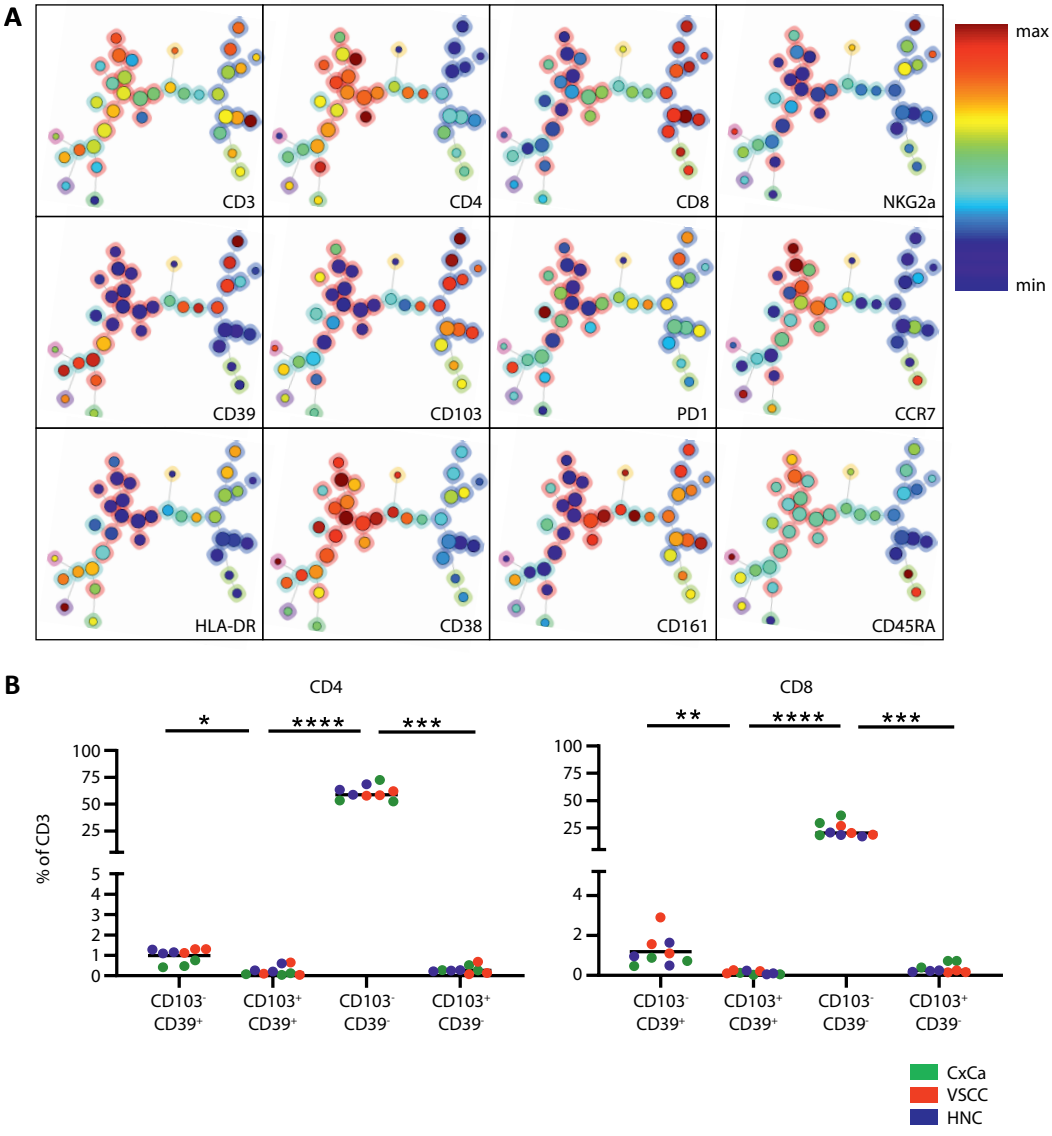

Supplemental figure 1. CD39 is expressed by CD8+ and CD4+ TIL in different types of cancer. Cryopreserved single cell tumor digests of patients with CxCa, VSCC and OPSCC (*n*=9, *n*=10 and *n*=11, respectively) were analyzed by 13-parameter flow cytometry analysis. Data was analyzed by FlowSOM analysis in cytobank. Minimum Spanning Trees (MST) displaying the expression levels of the indicated markers are depicted (A). Intensities are given in a color range from blue (min) to red (max). Cryopreserved PBMC samples of patients with CxCa, VSCC and OPSCC (*n*=3 each) were analyzed by 13-parameter flow cytometry analysis (B). Data was analyzed by manual gating DIVA software. Graphs depicting the percentage of $CD39^+CD103^-$, $CD39^+CD103^+$, $CD39^-CD103^-$ and $CD39^-CD103^+$ $CD4^+$ (left) and $CD8^+$ (right) T cells within CxCa (green), VSCC (red) and OPSCC (blue) patients. **p*<0.05, ***p*<0.01, ****p*<0.001, and *****p*<0.0001.

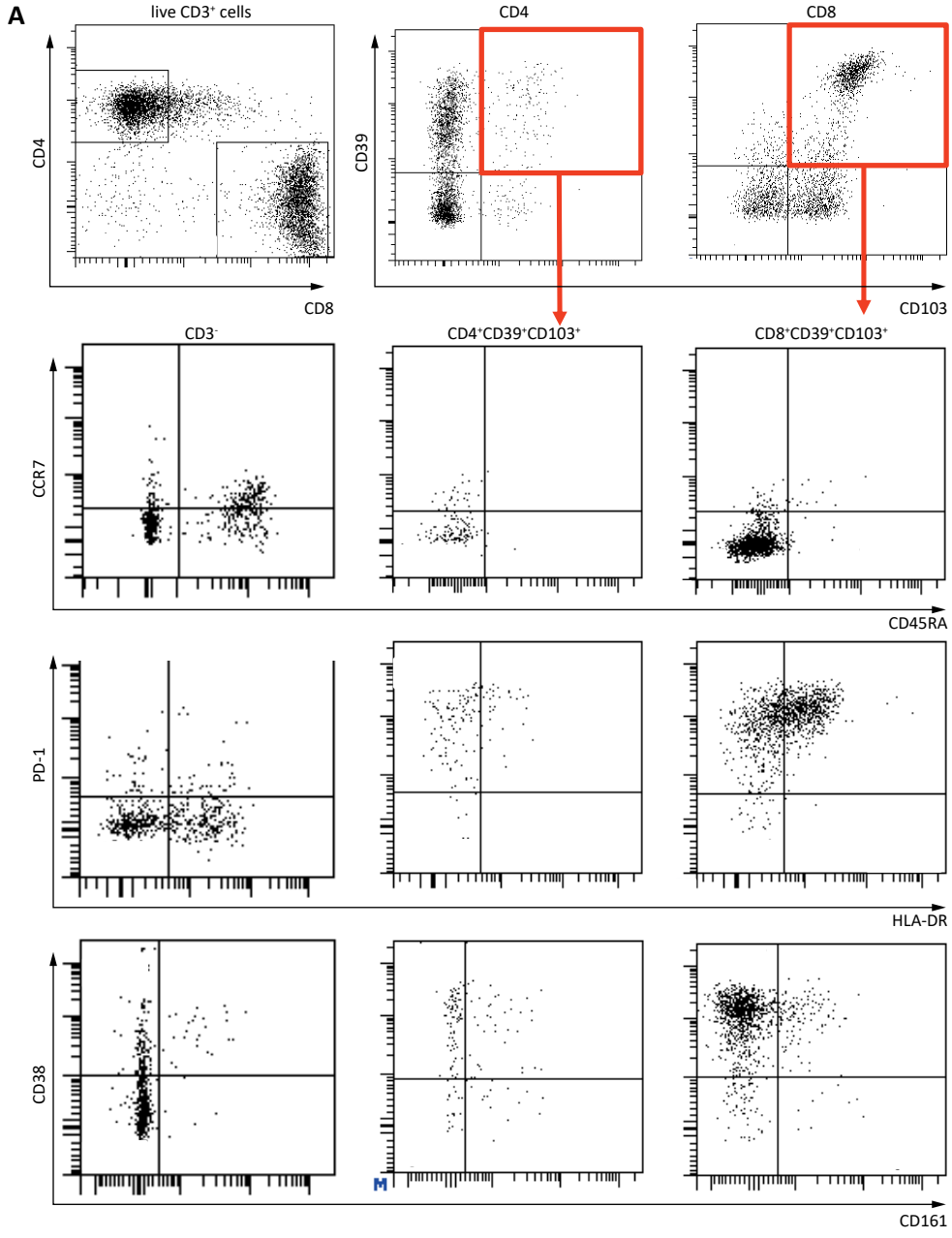

Supplemental figure 2. Gating strategy of *ex vivo* tumors. Singlets were gated on FSC-H/FSC-A properties, after which dead cells were excluded through gating on yellow amine reactive dye-negative cells (A). Next, $CD3^+$ T cells were selected, which were further divided based on CD4 and CD8 expression. Next, $CD39^+CD103^-$, $CD39^+CD103^+$, $CD39^-CD103^-$ and $CD39^-CD103^+$ cells were gated and further characterized based on the expression of CCR7, CD45RA, PD1, HLA-DR, CD38, CD161 and NKG2A. As an example, the gating strategy is shown for the reference population ($CD3^-$ cells, left panel) and $CD4^+CD39^+CD103^+$ (middle panel) and $CD8^+CD39^+CD103^+$ cells (right panel). (B) Gating example for determination of the mean fluorescence of PD-1 and HLA-DR for $CD3^-$ (left; reference gate), $CD4^+CD39^+CD103^+$ (middle panel) and $CD8^+CD39^+CD103^+$ cells (right panel).

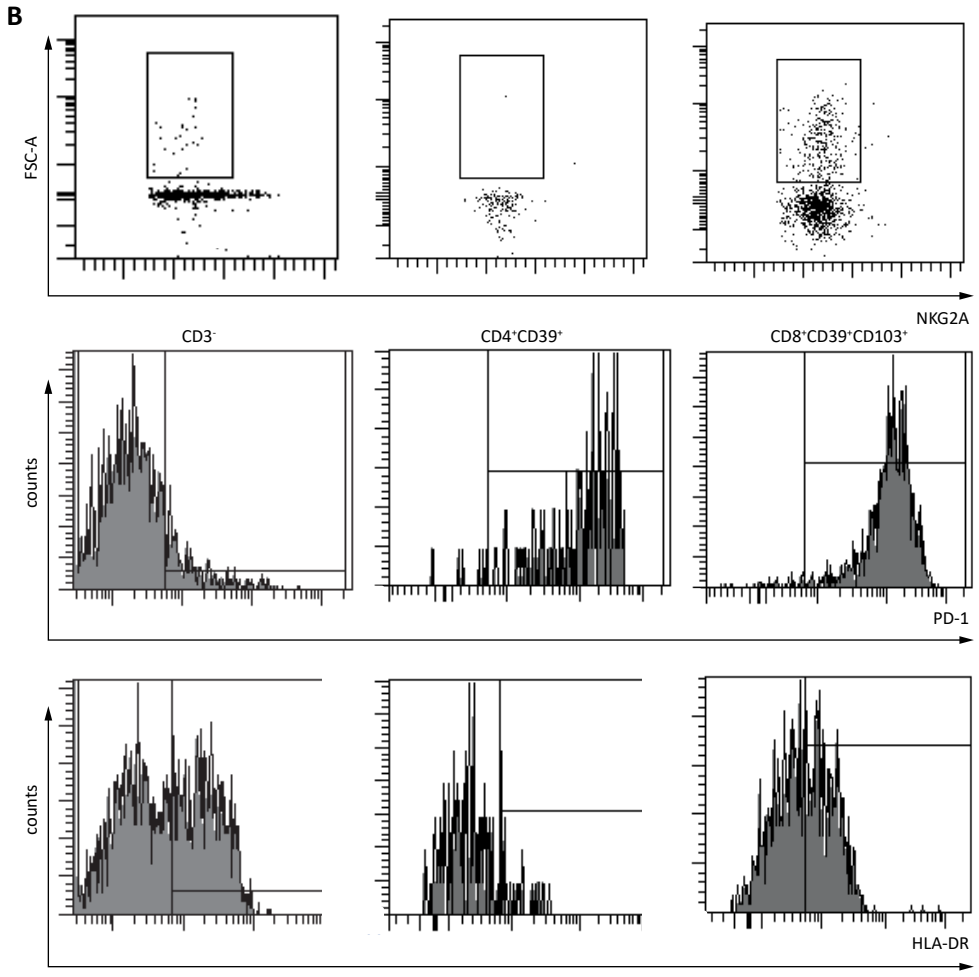

Supplemental figure 2. Continued

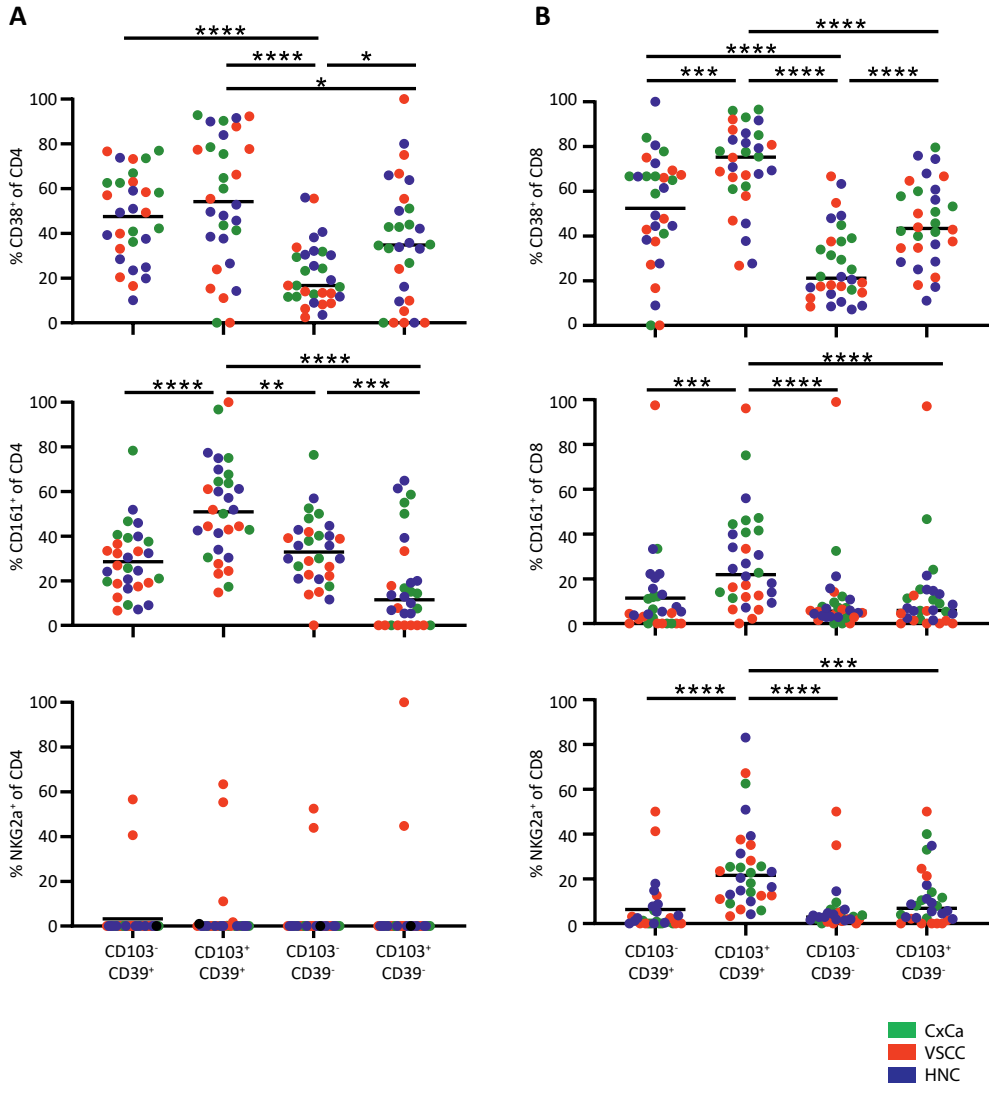

Supplemental figure 3. CD39⁺ subpopulations in TIL. Cryopreserved single cell tumor digests of patients with CxCa, VSCC and OPSCC were analyzed by 13-parameter flow cytometry analysis. Graphs depicting the percentage of CD38 (top), CD161 (middle) and NKG2a (bottom) within CD39⁺CD103⁻, CD39⁺CD103⁺, CD39⁻CD103⁻ and CD39⁻CD103⁺ CD4⁺ (A) and CD8⁺ (B) T cells for CxCa (green), VSCC (red) and OPSCC (blue) patients. Graphs depicting the mean fluorescence of PD-1 (top) and HLA-DR (bottom) within CD39⁺CD103⁻, CD39⁺CD103⁺, CD39⁻CD103⁻ and CD39⁻CD103⁺ CD4⁺ (C) and CD8⁺ (D) T cells for CxCa (green), VSCC (red) and OPSCC (blue) patients. Staining example (left) and graph (right) displaying the CD25 and Foxp3 expression within CD4⁺CD39⁺ cells in tumor (*n*=4; two VSCC and two CxCa patients) and blood (*n*=9 ; three VSCC, CxCa and OPSCC patients, (E)). Mean percentage of CD25⁺Foxp3⁺ regulatory T cells (Tregs, red), CD25⁺Foxp3⁻ activated non-Tregs (blue), CD25⁻Foxp3⁺ non-Tregs (green) and CD25⁻ Foxp3⁻ non-Tregs (yellow) is depicted. **p*<0.05, ***p*<0.01, ****p*<0.001, and *****p*<0.0001.

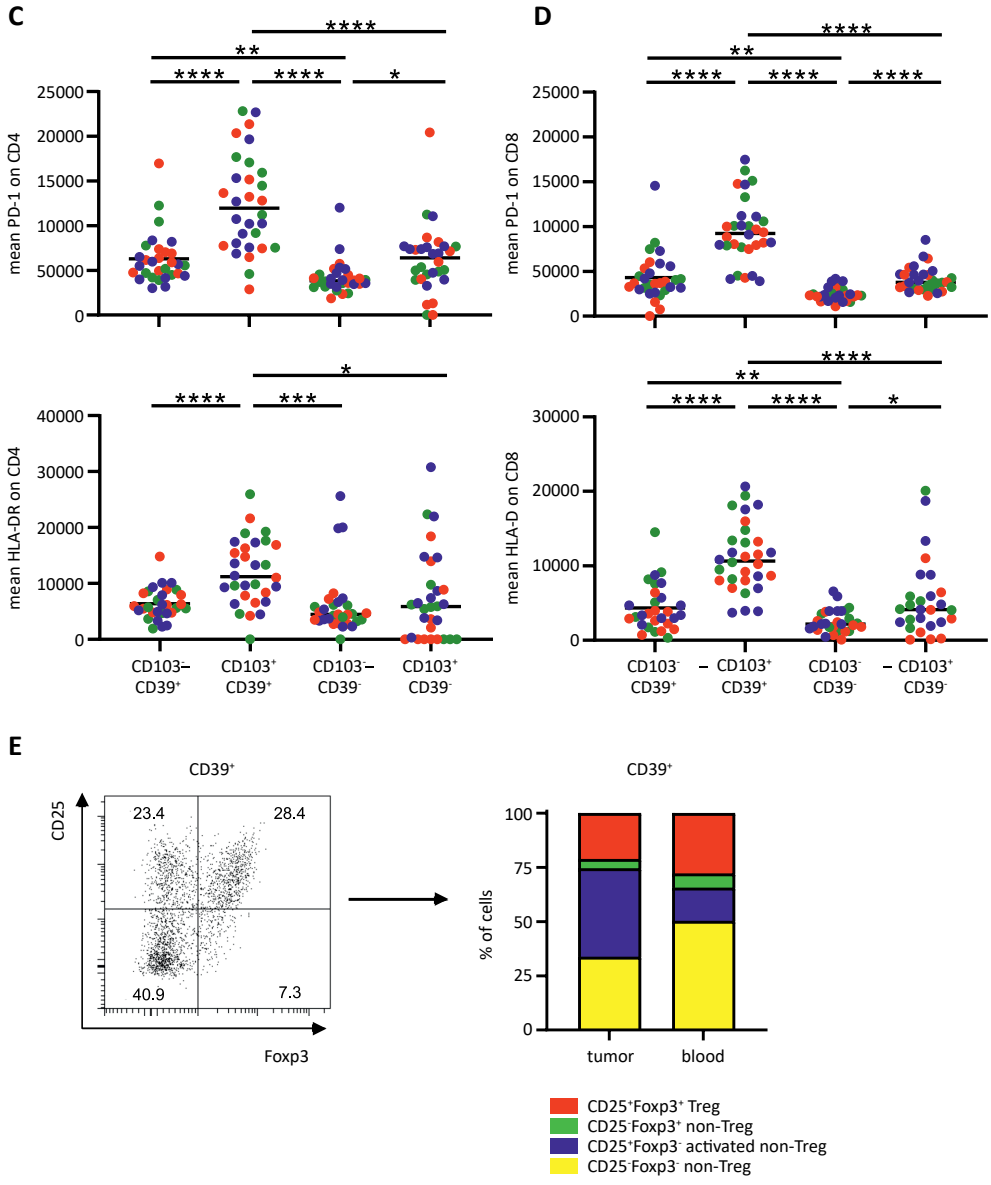

Supplemental figure 3. Continued

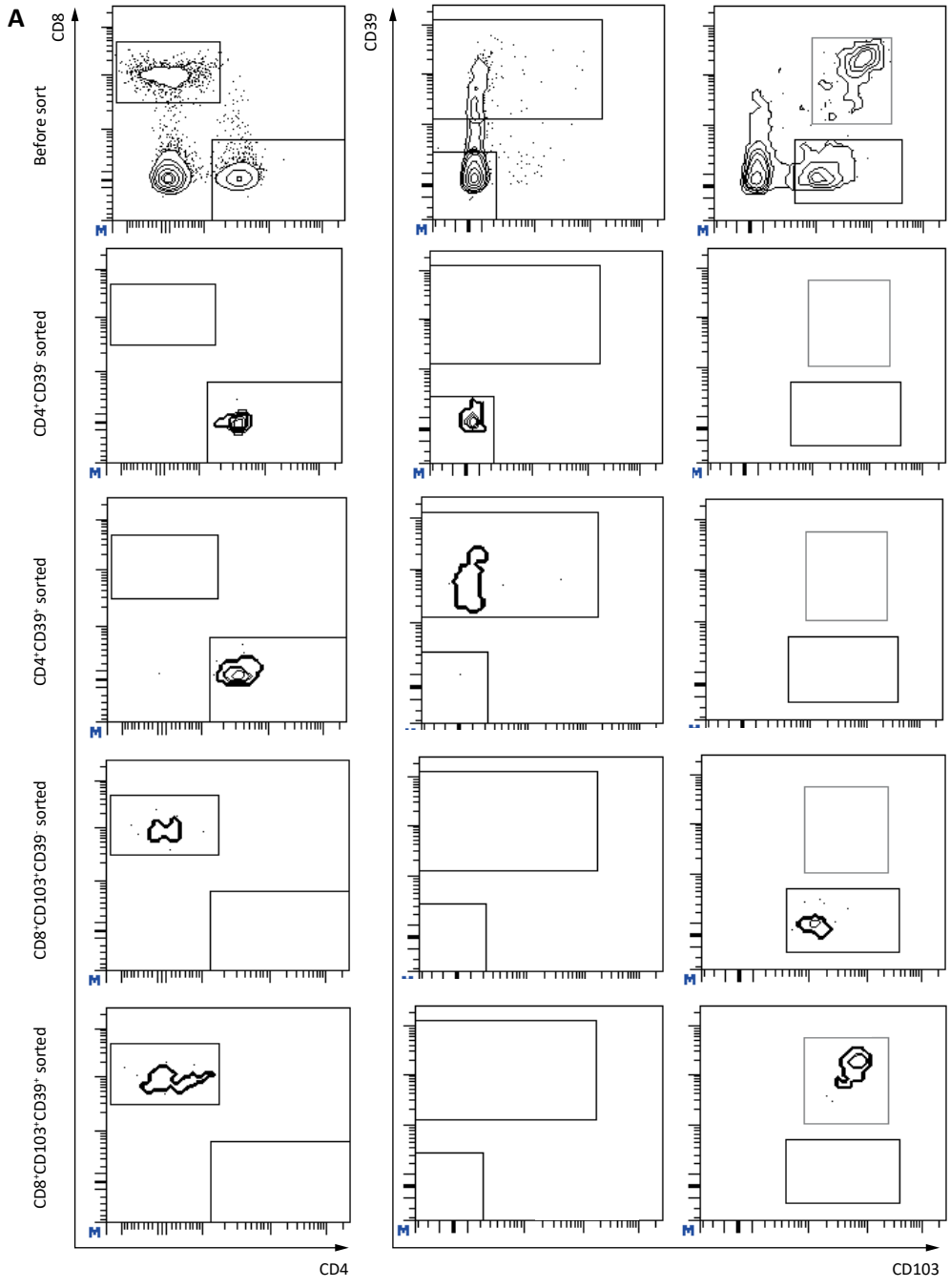

Supplemental figure 4. Gating strategy for sorting subpopulations. Singlets were gated on FSC/SSC properties, after which dead cells were excluded through gating on a live/dead marker. Next, $CD4^+$ and $CD8^+$ T cells were selected and where further subdivided based on the expression of CD39 and CD103. When enough cell of the populations of interest were sorted, a purity check was performed. Data given are sorting results from representative donor.

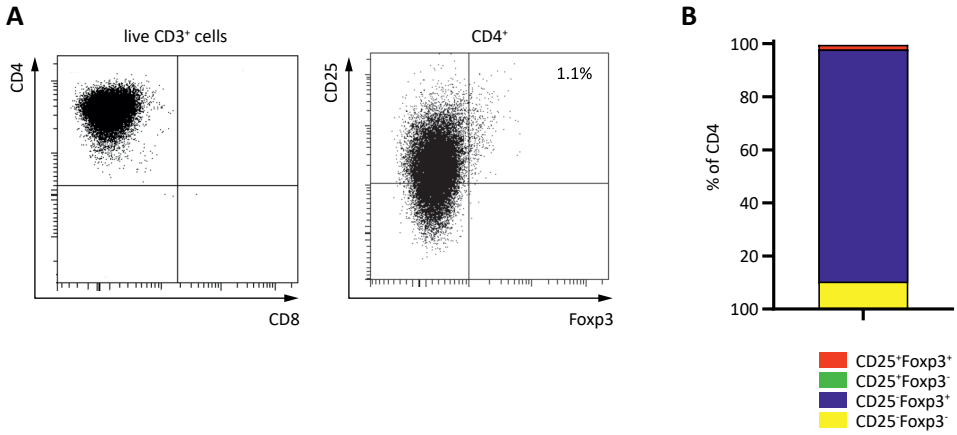

Supplemental figure 5. Expanded CD4$^+$CD39$^+$ cells do not express Foxp3. Singlets were gated on FSC-H/FSC-A properties, after which dead cells were excluded through gating on yellow amine reactive dye-negative cells. Next, CD3$^+$ T cells were selected, which were further divided based on CD25 and Foxp3 expression. Gating example is depicted for a representative TIL culture (A). Graph displaying the mean percentage of CD25$^+$Foxp3$^+$ (red), CD25$^+$Foxp3$^-$ (blue), CD25$^-$Foxp3$^+$ (green) and CD25$^-$Foxp3$^-$(yellow) for 10 TIL cultures (B).

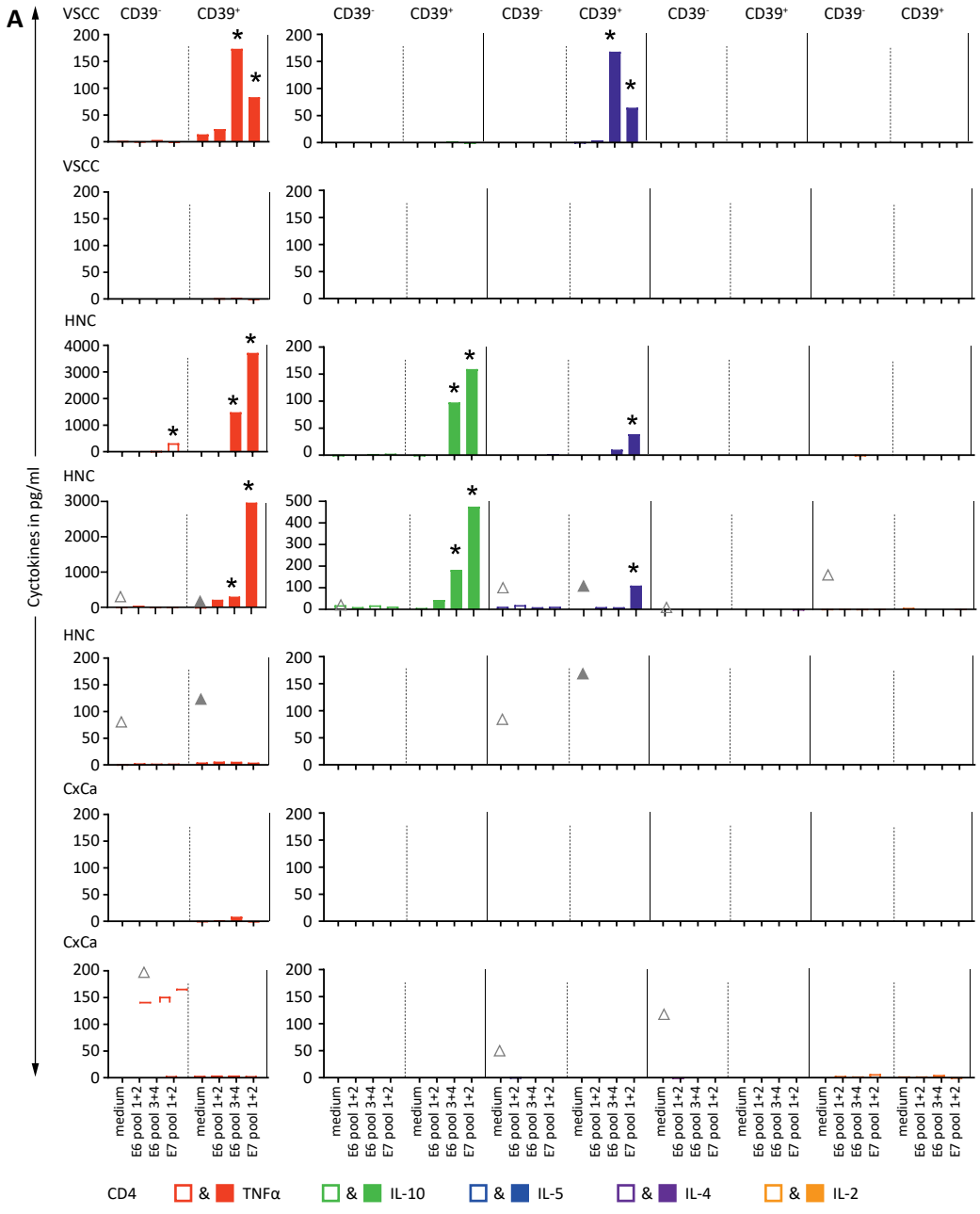

Supplemental figure 6. HPV-specific reactivity was almost exclusively detected amongst CD4$^+$CD39$^+$ and CD8$^+$CD39$^+$CD103$^+$ TIL. Graphs displaying the TNFα (left; red) and IL-10 (green), IL-5 (blue), IL-4 (purple) and IL-2 (orange) production of CD4$^+$CD39$^-$ and CD4$^+$CD39$^+$ TIL (A) and CD8$^+$CD39$^-$CD103$^+$ and CD8$^+$CD39$^+$CD103$^+$ TIL (B) in response to medium or HPV16 or HPV18 E6 (pool 1+2 and 3+4) and E7 (pool 1+2)-loaded autologous monocytes for seven HPV-associated SCC (*n*=2 VSCC, *n*=3 OPSCC, *n*=2 CxCa from top to bottom). Cytokine production in response to PHA, which served as a positive control, is depicted with the triangles. Positive cytokine production, which is defined as at least twice above that of the medium stimulated cells, is indicated by the black asterisk.

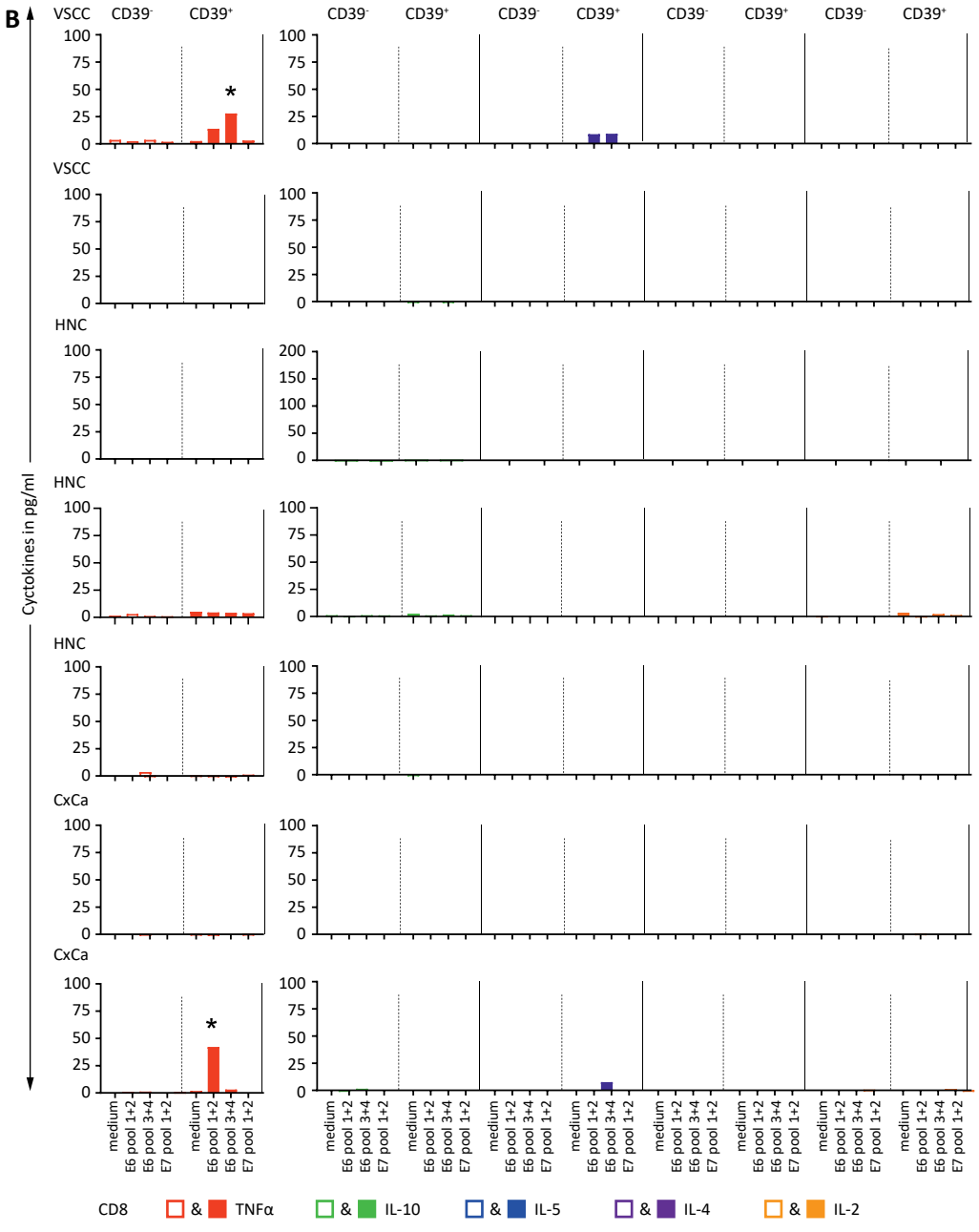

Supplemental figure 6. Continued

Supplemental table 1. Antibody panels.

	Antibody	Antigen	Fluorochrome	Clone	Supplier
Sort panel	1	CD4	AlexaFluor700	RPA-T4	BD Biosciences
	2	CD8	BB700	HIT8a	BD Biosciences
	3	CD39	BV421	A1	Biolegend
	4	CD103	BV605	Ber-ACT8	Biolegend
	5	Live/dead	Near-IR	-	ThermoFisher Scientific
Flowcytometry panel 1	1	CD3	PerCP-Cy5.5	2D1	BD Biosciences
	2	CD4	AlexaFluor700	RPA-T4	BD Biosciences
	3	CD8	BB700	HIT8a	BD Biosciences
	4	CD39	BV421	A1	Biolegend
	5	CD103	BV605	Ber-ACT8	Biolegend
	6	CD45RA	APC-H7	HI100	BD Biosciences
	7	CCR7	AlexaFluor488	G043H7	Biolegend
	8	CD161	PE	HP-3G10	Biolegend
	9	CD38	BV650	HB-7	Biolegend
	10	HLA-DR	V500	G46-6	BD Biosciences
	11	PD-1	PE-Cy7	EH12.2H7	Biolegend
	12	NKG2a	APC	Z199	Beckman Coulter
	13	Live/dead	Fixable yellow	-	Thermofisher scientific
Flowcytometry panel 2	1	CD3	BV510	UCHT1	Biolegend
	2	CD4	AF700	RPA-T4	BD Biosciences
	3	CD127	BV650	A019D5	Biolegend
	4	CD25	PE-Cy7	2A3	BD Biosciences
	5	CD45RA	APC-H7	HI100	BD Biosciences
	6	CD8	BB700	HIT8a	BD Biosciences
	7	CD39	BV421	A1	Biolegend
	8	PD-1	PE	MIH4	BD Biosciences
	9	CD103	BV605	Ber-ACT8	Biolegend
	10	Foxp3	PE-CF594	259D/C7	BD Biosciences
	11	Ki67	FITC	20raj1	eBiosciences
	12	Helios	APC	22F6	Biolegend
	13	Live/dead	Fixable yellow	-	Thermofisher scientific

Supplemental table 2. Expansion rates.

Number of cells t=0 days	<1.000	1.000-2.500	2.500-5.000	5.000-7.500	7.5000-10.000	>10.000-100.000
Expansion round 1 average total cells (min-max)	2.846.000 (1.380.000 - 4.300.000)	5.900.000 (1.650.000 - 6.570.000)	9.950.000 (1.200.000 - 11.900.000)	4.870.000 (1.900.000 - 10.740.000)	3.010.000 (1.050.000 - 4.280.000	15.431.250 (435.000 - 68.300.000)
Number of cells t=23 days	200.000	400.000	800.000			
Expansion round 2 average total cells (min-max)*	7.850.000 (5.600.000 – 10.100.000)	81.613.882 (10.700.000 – 153.900.000)	10.700.000 (5.600.000 – 14.000.000)			

*After expansion round 1, cells were harvested and counted. Before re-stimulation for expansion round 2.400.000 cells/condition were cultured. Two conditions had a low number of cells, for which 200.000 cells/condition were cultured. Three other conditions did not expand sufficiently, and in the second expansion round 800.000 cells/condition were cultured.